The reactions $CH_nD_{4-n}+OH \rightarrow P$ and $CH_4+OD \rightarrow CH_3+HOD$ as a test of current direct dynamics multicoefficient methods to determine variational transition state rate constants. II

Laura Masgrau, Àngels González-Lafont, and José M. Lluch[a)]
Departament de Química, Universitat Autònoma de Barcelona, 08193 Bellaterra, Barcelona, Spain

(Received 23 April 2001; accepted 14 June 2001)

In this paper we have carried out a test of current multilevel electronic structure methods to give accurate rate constants for the reactions $CH_nD_{4-n}+OH \rightarrow P$ and for the reaction of methane with OD. These multilevel methods are single-point energy techniques designed as general parametrizations for extrapolation to the full configuration interaction limit and, in some cases, to attain also the infinite basis set limit. By means of variational transition state theory including multidimensional tunneling corrections, the rate constants for these reactions, over a wide range of temperatures, have been computed using two recently developed multicoefficient schemes for extrapolating correlated electronic structure calculations: multicoefficient scaling all correlation (MCSAC) and multicoefficient correlation methods (MCCM). For comparison purposes, we have also evaluated the same rate constants using two other multilevel extrapolation techniques, namely, the multicoefficient quadratic configuration interaction (MC-QCISD) method and the complete basis set extrapolation model for free radicals (CBS-RAD). Two dual-level direct dynamics techniques have been employed within the scheme of variational transition state theory: the interpolated single-point energy corrections (ISPE) and the interpolated optimized corrections (IOC), with the purpose to analyze the importance of correcting a low level potential energy surface with the optimizations of the stationary points carried out at the highest computational level affordable. We have shown that the so-called MCCM-CCSD(T)-1*sc* multilevel scheme provides the best results for the set of reactions studied. A slight difference from the experimental rate constants still persists, specially at the lowest temperatures, although we think that the best theoretical rate constants of the present paper are accurate enough for most of the practical applications. However, the kinetic isotope effects (KIEs) are not so well reproduced because the deviations of the individual theoretical rate constants from the experimental ones, although being very small, do not go in the same direction and these errors are reinforced when the corresponding KIE is calculated. © *2001 American Institute of Physics.* [DOI: 10.1063/1.1389848]

I. INTRODUCTION

Ab initio electronic structure methods have attained a degree of accuracy on the calculation of bond energies and heats of formation of small systems comparable or, in some cases, even better than experiment. However, there are still many difficulties in the theoretical calculation of barrier heights, especially in the case of radical–molecule reactions because the transition state is an open-shell system.[1–9] The correct determination of classical potential energy barriers is the first condition that has to be fulfilled in order to obtain accurate rate constant values using, for example, transition state theory. Consequently, the theoretical calculation of precise values for the rate constants of radical–molecule reactions is still a challenging task for current computational methods.

In the previous paper,[9] hereafter called paper I, we analyzed the capability of several electronic structure methods, which stand for the present state of the art of monoreference electronic structure theory, to give accurate rate constants of radical–molecule reactions when these electronic calculations were combined with variational transition state theory including multidimensional tunneling calculations[10,11] (VTST/MT). As a test, we selected the six following abstraction reactions in the temperature range 200–1500 K:

$$OH+CH_4 \rightarrow H_2O+CH_3, \quad \text{(R1)}$$

$$OH+CH_3D \rightarrow H_2O+CH_2D \quad \text{and} \quad HDO+CH_3, \quad \text{(R2)}$$

$$OH+CH_2D_2 \rightarrow H_2O+CHD_2 \quad \text{and} \quad HDO+CH_2D, \quad \text{(R3)}$$

$$OH+CHD_3 \rightarrow H_2O+CD_3 \quad \text{and} \quad HDO+CHD_2, \quad \text{(R4)}$$

$$OH+CD_4 \rightarrow HDO+CD_3, \quad \text{(R5)}$$

$$OD+CH_4 \rightarrow HDO+CH_3. \quad \text{(R6)}$$

The results of paper I demonstrated that variational effects and tunneling corrections have to be included in the calculation of the rate constants of these abstraction reactions. However, and although our results were quite good from a quantitative point of view, we did not match exactly the available experimental rate constants for these reactions.[11–18] The best quantitative results were obtained

a)Author to whom correspondence should be addressed.

with a direct dynamics interpolated single-point energy correction[19] (ISPE) calculation at CCSD(T)-SAC/cc-pVTZ//MP2/cc-pVTZ level [SAC (Refs. 20–22) stands for scaling all of the correlation energy]. SAC is one of the available multilevel single-point energy techniques[23–26] based on linearly combining a series of calculations at different levels of electronic correlation in order to extrapolate to the full configuration interaction limit. These multilevel calculations are affordable even for medium-sized systems and in many cases have shown more accuracy, at least in thermochemical calculations, than the highest single-level computationally feasible calculations. The overall methodology for SAC is to scale with a unique factor all of the correlation energy that comes from a given level of correlation energy treatment, but using a single basis set. However, the different components of the correlation energy may need different scaling factors. Motivated by the SAC procedure and another extrapolation procedure, namely the *ab initio* infinite basis set (IB) method,[27–29] Truhlar and co-workers have recently developed two new methodologies within the field of general parametrization for semiempirical extrapolation approaches. These new electronic structure methods are known as multicoefficient scaling all correlation (MCSAC) and multicoefficient correlation methods[30–34] (MCCM). In these two extrapolation schemes, variable coefficients or scaling factors can be assigned to the different components of the correlation energy. The MCCM approaches, in addition, are designed to attain the infinite basis set limit.

The main purpose of this work is to continue with the analysis started in paper I on the entitled reactions. In the present study, the capability of several MCSAC and MCCM methods to give quantitative rate constant values for reactions (R1)–(R6) is examined in detail for a wide range of temperatures. All of these methods were designed as single-point energy techniques. That is, molecular geometries are optimized at a lower level of electronic correlation with a small- or medium-sized basis set, and a multilevel single-point energy calculation is made based on those optimized geometries. On the other hand, we have intended to assess the influence of the chosen geometric optimization in the multilevel single-point energy calculations and, consequently, in the results for the rate constants. Then, we also present some calculations carried out with two other multilevel methods based on optimized geometries at a different level of electronic correlation or/and with a different kind of basis set than in the MCSAC and in the MCCM methods. In addition, a comparison is made between two dual-level direct dynamics techniques based on correcting a low level potential energy surface (PES) with electronic structure information calculated at a higher level. These two dual-level approaches developed in the field of VTST are the ISPE direct dynamics interpolated method, that only accounts for single-point energy corrections, and the interpolated optimized corrections (IOC) methodology[35,36] that accounts for corrections in the classical potential energy, in the geometries and in the frequencies.

II. METHOD OF CALCULATION

In this section we will first explain the electronic structure calculations and the direct dynamics VTST/MT calculations for the perprotio reaction (R1), and later we will comment on the isotopic substituted reactions (R2)–(R6). In this section, several details of the calculations will be skipped because they were already described in paper I.

A. Electronic structure calculations

Four different multilevel electronic methods have been used in the present work: the multicoefficient scaling all correlation method (MCSAC), the multicoefficient correlation method (MCCM), the multicoefficient quadratic configuration interaction with single and double excitations[37] (MC-QCISD), and the complete basis set extrapolation model for free radicals[38] (CBS-RAD), which is a modification of the CBS-Q method.[39] All of them use geometries, gradients, and second derivatives at one electronic level, and the classical energies come from a linear combination of single-point energy calculations at these geometries. As it will be detailed below, other two energy contributions may also be added in the final expression of the multilevel classical energy.

1. Stationary point calculations

For the MCSAC and MCCM calculations, stationary point geometries, first and second derivatives at second-order Møller–Plesset perturbation theory[40,41] (MP2) based on restricted Hartree–Fock (RHF) or unrestricted Hartree–Fock[40] (UHF) wave functions for closed-shell and open-shell systems, respectively, and with a full electron correlation treatment, have been taken from our previous work on the entitled reactions. The basis set used in paper I, and also adopted here, was a correlation-consistent polarized-valence triple zeta[42] (cc-pVTZ) basis set of Dunning with pure *d* and *f* functions. Although the development of these methods was made with MP2(fc)/cc-pVDZ geometries, first and second derivatives, Truhlar and co-workers[37] pointed out that the methods should be independent of the electronic level used for geometry optimization. For simplicity, we will omit the geometry specification in the electronic level notation, assuming then that for both of these methods the geometries, first and second derivatives are at MP2(full)/cc-pVTZ level of theory. Otherwise, the electronic level chosen for the optimization and the frequency calculation will be clearly stated.

The MCSAC method represents an attempt to extrapolate to the full configuration interaction (FCI) limit by scaling all of the correlation energy that comes from a given level of correlation energy treatment, using a single basis set. In particular, we have used the MCSAC-CCSD(T)/cc-pVTZ scheme [where CCSD(T) stands for the coupled cluster method including single and double excitations and a perturbative estimate of the effect of triple excitations].[43] The single-point energy can be written as

$$E[\mathrm{MCSAC-CCSD(T)/cc\text{-}pVTZ}] = E(\mathrm{HF/cc-pVTZ}) + c_1\Delta E(\mathrm{MP2|HF/cc\text{-}pVTZ}) + c_2\Delta E(\mathrm{CCSD|MP2/cc\text{-}pVTZ}) + c_3\Delta E[\mathrm{CCSD(T)|CCSD/cc\text{-}pVTZ}] + E_{\mathrm{SO}} + E_{\mathrm{CC}}, \quad (1)$$

where $\Delta E(\mathrm{M1|M2/B}) = E(\mathrm{M1/B}) - E(\mathrm{M2/B})$ (M and B denote electronic level and basis set, respectively), c_i are coefficients, CCSD is the notation for the coupled cluster method including single and double excitations, E_{SO} and E_{CC} are the spin–orbit[23] and core-correlation[44] contributions, respectively.

The MCCM method not only attempts to extrapolate to the FCI limit, but also to reach the infinite-basis limit. It combines the MCSAC strategy with the extrapolation of correlation-consistent basis sets for a given electron correlation level. Particularly, we have used the MCCM-CCSD(T) scheme in its Colorado version, which gives a single-point energy equal to

$$\begin{aligned} E[\mathrm{MCCM-CCSD(T)}] &= c_1E(\mathrm{HF/cc\text{-}pVDZ}) + c_2\Delta E(\mathrm{HF/cc\text{-}pVTZ|cc\text{-}pVDZ}) \\ &+ c_3\Delta E(\mathrm{MP2|HF/cc\text{-}pVDZ}) \\ &+ c_4\Delta E(\mathrm{MP2|HF/cc\text{-}pVTZ|cc\text{-}pVDZ}) \\ &+ c_5\Delta E(\mathrm{CCSD|MP2/cc\text{-}pVDZ}) \\ &+ c_6\Delta E(\mathrm{CCSD|MP2/cc\text{-}pVTZ|cc\text{-}pVDZ}) \\ &+ c_7\Delta E[\mathrm{CCSD(T)|CCSD/cc\text{-}pVDZ}] \\ &+ c_8\Delta E[\mathrm{CCSD(T)|CCSD/cc\text{-}pVTZ|cc\text{-}pVDZ}] + E_{\mathrm{SO}} \\ &+ E_{\mathrm{CC}}, \end{aligned} \quad (2)$$

where

$$\Delta E(\mathrm{M1/B1|B2}) = E(\mathrm{M1/B1}) - E(\mathrm{M1/B2}),$$

$$\Delta E(\mathrm{M1|M2/B1|B2}) = [E(\mathrm{M1/B1}) - E(\mathrm{M2/B1})] - [E(\mathrm{M1/B2}) - E(\mathrm{M2/B2})]$$

(M and B again indicate electronic method and basis set, respectively), cc-pVDZ is a correlation-consistent polarized-valence double zeta basis set of Dunning with pure d and f functions, and $\Delta E(\mathrm{M1|M2/B})$, c_i, E_{SO} and E_{CC} are analogous to those in Eq. (1).

Notice that for both MCSAC and MCCM methods all the single-point energy calculations are done with a frozen-core treatment of the correlation energy and, therefore, we need to add the E_{CC} correction. Moreover, the E_{SO} and E_{CC} terms can be included explicitly [like in Eqs. (1) and (2)] or can be implicit in the c_i ($i=1-3$ for MCSAC and 1–8 for MCCM) coefficients. Hence, we have different sets of c_i coefficients depending on how we introduce the spin–orbit and the core-correlation contributions. In the development of multicoefficient methods, the coefficients within each set were optimized to get accurate atomization energy values of a 49 or 82-molecule data set.

With the purpose of circumventing the calculation of the E_{CC} term at the saddle point, as it will be explained in the Results section, we have also calculated the MCSAC-CCSD(T)/cc-pVTZ and MCCM-CCSD(T) energies with a full electron correlation treatment [the CCSD(T)(full)/cc-pVTZ and MP2(full)/cc-pVTZ energies have been taken from paper I, and we have now calculated the CCSD(T)(full)/cc-pVDZ and MP2(full)/cc-pVDZ single-point energies].

The MC-QCISD method[37] is, in fact, a multicoefficient correlation method but based on basis sets using segmented contraction and having the same exponential parameters in the s and p spaces. The geometries and the zero-point energies (scaled by 0.9661) (Ref. 45) are calculated at the MP2(full)/6-31G(d) (Ref. 46) electronic level and the energy is given by

$$\begin{aligned} E(\mathrm{MC-QCISD}) &= c_0E[\mathrm{HF/6-31G}(d)] \\ &+ c_1\Delta E[\mathrm{MP2|HF/6-31G}(d)] \\ &+ c_2\Delta E[\mathrm{MP2/MG3|6-31G}(d)] \\ &+ c_3\Delta E[\mathrm{QCISD|MP2/6-31G}(d)], \end{aligned} \quad (3)$$

where all the single-point energy calculations have a frozen-core treatment, and the spin–orbit and core-correlation contributions are implicit in the c_i coefficients (optimized to get accurate atomization energy values of the 82-molecule data set). The MG3 basis set[34,47] is also called G3MP2large basis set,[48] and it is essentially an improved[47] version of the 6-311++G($3d2f$,$2df$,$2p$) basis set.

For the CBS-RAD stationary point calculations we have used the CBS-RAD(Q,Q) (Ref. 38) procedure, in which the geometry and zero-point energies (scaled by 0.9776) (Ref. 45) are obtained at the QCISD(fc)/6-31G(d) level of theory.[49]

At the MP2(full)/cc-pVTZ stationary points, single-point energy calculations with the MC-QCISD and with the CBS-RAD(Q,Q) multilevel methods are also presented.

Motivated by the geometry deviation between the low level saddle-point structures and the geometry of maximum classical energy on the corresponding high level classical energy profiles, we decided to improve the level of the geometry optimization. So, the stationary points for the perprotio reaction have also been located and characterized at the QCISD(fc)/cc-pVTZ level of theory. Multilevel single-point energy calculations were then carried out for these stationary points at the MCCM-CCSD(T)//QCISD(fc)/cc-pVTZ level.

For comparison, we have also taken from the literature several saddle point structures located at different electronic levels.[4,8]

2. Reaction path calculations

As it will be described in the dynamical calculations section, we have carried out dual-level dynamics calculations. Unless otherwise specified, the low level minimum energy path[50] (MEP) has been taken from paper I. It consists in a total of 35 nonstationary points (geometries, gradients, and Hessians), calculated at the MP2(full)/cc-pVTZ level of

theory, from $s=-2.20$ bohr to $s=0.50$ bohr (where s denotes the distance along the MEP in an isonertial mass-scaled coordinate system[51] with a scaling mass equal to 1 amu, with $s=0$ at the saddle point, s negative on the reactant side of the saddle point and positive on the product side).

Single-point energy calculations at the MCSAC-CCSD(T)/cc-pVTZ and MCCM-CCSD(T) levels, with both a frozen-core and a full electron correlation treatments, have been made at a small number of nonstationary point geometries along the MP2(full)/cc-pVTZ MEP, to correct the classical energy profile for the dynamical calculations. The location of five of these points along the MEP corresponds to the one chosen in our previous work, that is at s values of -0.900, -0.200, -0.051, $+0.031$, and $+0.051$ bohr. The location of the rest of nonstationary points used, if any, will be indicated later for each particular methodology.

We have also located the geometry of maximum MC-QCISD energy along the MP2(full)/6-31G(d) MEP, which will be denoted as Max{MC-QCISD}//MEP{MP2(full)/6-31G(d)} and the structure of maximum CBS-RAD(Q,Q) energy along the QCISD(fc)/6-31G(d) MEP, namely Max{CBS-RAD(Q,Q)}//MEP{QCISD(fc)/6-31G(d)}. Additionally, we have calculated CBS-RAD and MC-QCISD single-point energies at a small number of points along the MP2(full)/cc-pVTZ MEP. We will refer to these calculations as CBS-RAD//MP2(full)/cc-pVTZ and MC-QCISD/MP2(full)/cc-pVTZ, respectively.

We have carried out all the multilevel energy calculations involved in the MCSAC-CCSD(T)/cc-pVTZ, MCCM-CCSD(T), and MC-QCISD schemes with the MULTILEVEL 2.1 code.[52] For the rest of single-point energy calculations and the geometry optimizations, we have used the GAUSSIAN 94 system of programs.[53]

B. Dynamical calculations

Canonical variational transition state theory[51,54–58] (CVT) plus multidimensional tunneling (MT) contributions have been used to calculate the rate constants in the interval 200–1500 K. The small-curvature tunneling[59] (SCT) semiclassical adiabatic ground-state approximation has been used to correct for tunneling. The CVT/SCT rate constant is given by

$$k^{\mathrm{CVT/SCT}}(T,s_*)=\kappa^{\mathrm{SCT}}(T)\frac{\sigma k_B T}{h}\frac{Q^{\mathrm{GT}}(T,s_*)}{Q^R(T)}\times\exp(-V_{\mathrm{MEP}}(s_*)/k_B T), \tag{4}$$

where $\kappa^{\mathrm{SCT}}(T)$ is the SCT transmission coefficient, s_* denotes the value of s at the free energy maximum along the MEP at temperature T, σ is the symmetry factor,[60] k_B is Boltzmann's constant, h is Planck's constant, $Q^R(T)$ and $Q^{\mathrm{GT}}(T,s_*)$ are the reactants and the generalized transition state partition functions per unit volume, respectively, excluding symmetry numbers for rotation, and $V_{\mathrm{MEP}}(s_*)$ is the classical potential energy at s_*.

As in our previous work, the reoriented dividing surface[61] (RODS) algorithm has been applied in order to improve the generalized frequencies along the low level MEP. The normal mode analysis has been performed in redundant internal coordinates[62] (six stretches, eight bends, and four torsions). All vibrations have been treated within the harmonic approximation except the internal rotational motion corresponding to the lowest mode at the saddle point and along the MEP which has been treated as a hindered rotor[63] (see paper I for details). We have assumed no low-lying excited state of the $^2A_1$ saddle point but we have included the $^2\Pi_{1/2}$ excited state (140 cm^{-1}) for OH, in the electronic partition functions.

Two dual-level direct dynamics procedures have been used: the interpolated single-point energy correction[20] (ISPE) and the interpolated optimized corrections (IOC) algorithms.[35,36]

For the MCSAC-CCSD(T)/cc-pVTZ and the MCCM-CCSD(T) electronic levels, the ISPE procedure has been applied. The MP2(full)/cc-pVTZ information (geometries and frequencies scaled by 0.9790) (Refs. 23, 45) has been used as the low level (LL). The MCSAC-CCSD(T)/cc-pVTZ and the MCCM-CCSD(T) classical energies of the stationary points and of several nonstationary points, were used as the high level (HL) information to correct for the energetics. For the MC-QCISD//MP2(full)/cc-pVTZ and CBS-RAD//MP2(full)/cc-pVTZ multilevel electronic methods, we have also carried out ISPE direct dynamics calculations using, again, the MP2(full)/cc-pVTZ MEP as the low level information (geometries and frequencies also scaled by 0.9790) and the corresponding multilevel single-point classical energies at the stationary points and at several nonstationary points as the high level (HL) information to correct for the energetics.

For the MC-QCISD, CBS-RAD(Q,Q), and MCCM-CCSD(T)//QCISD(fc)/cc-pVTZ multilevel methods we have applied the IOC scheme. In this scheme, the LL MEP [MP2(full)/cc-pVTZ in this work] is corrected with HL energies, moments of inertia, and frequencies calculated only at the stationary points. Although Truhlar and co-workers have renamed this general scheme as interpolated optimized corrections (IOC), we prefer to call it here intermediate-IOC because we have not used as HL geometries the ones resulting from the optimization with the full multilevel energy expression [that is, what Truhlar and co-workers[64] would name as MC-QCISD//ML, CBS-RAD(Q,Q)//ML or MCCM-CCSD(T)//ML, "//ML" stands for each multilevel optimization] but the geometries and frequencies calculated at the MP2(full)/6-31G(d) level (in the MC-QCISD scheme), at the QCISD(fc)/6-31G(d) level [in the CBS-RAD(Q,Q) approach] and at the QCISD(fc)/cc-pVTZ level (in the MCCM-CCSD(T)//QCISD(fc)/cc-pVTZ method).

We have used the POLYRATE 8.5.1 code[65] for all the dynamical calculations.

C. Isotopically substituted reactions

As we explained in paper I, no extra electronic structure calculations are needed for the isotopically substituted reactions when applying the RODS algorithm. Thus, for reactions (R2)–(R6) we have taken the perprotio MEP as the reaction path.

Reactions (R2), (R3), and (R4) involve more than one isotopically nonequivalent channel depending on the position

of the deuterium atom(s) in the molecule. Consequently, the competitive canonical unified statistical theory[66] (CCUS) has been applied (see paper I for more details), and the final rate constant, $k(T)$, is given by

$$k(T)=\sum_i k_i(T), \tag{5}$$

where i is the number of isotopically nonequivalent channels and $k_i(T)$ is the CVT/SCT rate constant in Eq. (4) calculated for each of these channels. In Table II of paper I, the symmetry numbers for the different channels are given.

III. RESULTS AND DISCUSSION

In this section, electronic and dynamical calculations are presented together to facilitate analysis, since the rate constants are very sensitive to any change on the potential energy surface (PES). First, ISPE calculations at the MCSAC-CCSD(T)/cc-pVTZ and at the MCCM-CCSD(T) electronic levels, for (R1) and (R5), are commented. Later, we present additional ISPE results for (R1) based on the CBS-RAD//MP2(full)/cc-pVTZ and MC-QCISD//MP2(full)/cc-pVTZ electronic methods. Moreover, intermediate-IOC calculations for (R1) based on the CBS-RAD(Q,Q) and the MC-QCISD methods are also presented. Finally, a comparison is made with the results obtained with the intermediate-IOC scheme using as high level information the MCCM-CCSD(T)//QCISD(fc)/cc-pVTZ electronic structure calculations. In the last subsection, the method that best reproduces both (R1) and (R5) experimental rate constants will be used to calculate the rate constants for (R2)–(R4) and (R6).

A. MCSAC-CCSD(T)/cc-pVTZ and MCCM-CCSD(T) ISPE calculations for (R1) and (R5)

These multilevel single-point energy calculations for (R1) were carried out at the MP2(full)/cc-pVTZ geometries from paper I. As we already explained in that previous paper, two van der Waals complexes were found on the MP2(full)/cc-pVTZ PES: one stationary structure on the reactant side and another in the exit channel. Although that, due to their location on the PES and to the size of the proton shift energy barrier, the kinetic reaction pathway for (R1)–(R6) can be thought at 0 K and at higher temperatures to take place through only one dynamical bottleneck corresponding to the hydrogen (or deuterium) abstraction process itself.

To include the core-correlation and spin–orbit contributions in Eqs. (1) and (2), there are several possibilities. Keeping the notation used in the MULTILEVEL package, we have

$1sc$ and $2sc$: E_{CC} and E_{SO} are included explicitly, as in Eqs. (1) and (2).

$2s$: E_{CC} is included implicitly in the coefficients and E_{SO} is included explicitly, so we only remove E_{CC} in Eqs. (1) and (2).

$2m$: E_{CC} and E_{SO} are included implicitly in the coefficients, so we delete them from Eqs. (1) and (2);

Number 1 or 2 indicate the 42 or 82-molecule data set used in the parametrization, respectively.

TABLE I. From left to right (all the energy values in kcal/mol)/: Multilevel method used in the ISPE calculations; multilevel classical potential energy at the MP2(full)/cc-pVTZ saddle point structure; value of s (in bohr) at which the maximum of the multilevel classical potential energy profile occurs; maximum of the multilevel classical potential energy profile; maximum of the multilevel adiabatic energy profile; multilevel classical energy of reaction. All the results refer to the (R1) reaction.

Multilevel method	$V^{\neq}$	$s(V_{max})$	V_{max}	ΔV_a^G	ΔV
MCSAC-CCSD(T)/cc-pVTZ-1sc	4.04	−0.15	4.20	4.93	−11.14
MCSAC-CCSD(T)/cc-pVTZ-2sc	5.52	−0.06	5.53	6.02	−12.00
MCSAC-CCSD(T)/cc-pVTZ-2s	4.86	−0.10	4.91	5.50	−12.35
MCSAC-CCSD(T)/cc-pVTZ-2m	5.38	−0.10	5.47	6.06	−12.21
MCCM-CCSD(T)-1sc	5.16	−0.01	5.16	5.53	−12.76
MCCM-CCSD(T)-2sc	5.47	0.00	5.47	5.65	−12.83
MCCM-CCSD(T)-2s	5.06	−0.01	5.06	5.36	−12.88
MCCM-CCSD(T)-2m	5.62	−0.01	5.62	6.00	−12.82

The ISPE direct dynamics calculations at the MCSAC-CCSD(T)/cc-pVTZ and the MCCM-CCSD(T) levels were carried out with these four possibilities to account for spin–orbit and core-correlation effects. We denote them by adding $1sc$, $2sc$, $2s$, $2m$ after MCSAC-CCSD(T)/cc-pVTZ or MCCM-CCSD(T). Before analyzing the results, two important issues must be pointed out. The first one is that in those cases where E_{SO} is explicitly given ($1sc$ and $2sc$), we have taken $E_{SO}=-0.2$ kcal/mol for the hydroxyl radical and $E_{SO}=0.0$ for the other stationary points and along the MEP, as they are closed-shell molecules or doublet molecules in the ^2A state, which have E_{SO} necessarily zero in the Russell–Saunders scheme. The second issue refers to the calculation of E_{CC}. A simple approximation of core-correlation effects at the equilibrium internuclear geometry is described in Ref. 44. However, at the saddle point structure and along the MEP we would need the dependence on geometry of the E_{CC} term, and then the calculation of E_{CC} turns out to be more complicated. To circumvent this difficulties, we have used the $1sc$ and $2sc$ sets of coefficients omitting the E_{CC} term in Eqs. (1) and (2), but calculating the single-point energies with a full electron correlation treatment.

Table I summarizes the results for the energetics of the (R1) reaction. In paper I we already commented the difficulties that single-level electronic methods have to give accurate exoergicities for hydrogen abstraction reactions. It seems that multilevel methods such as SAC, SEC, MCSAC, MCCM, CBS,... and specially the G2 family, have made a significant progress in this field. In Table I, the classical reaction energies (ΔV) go from −11.14 to −12.88 kcal/mol, with the best value obtained at the MCCM-CCSD(T)-2s level (−12.88 kcal/mol), if we compare to the experimental value estimated by Truhlar and co-workers (−13.49 kcal/mol).[67] For the MCSAC-CCSD(T)-1sc and -2s levels, two extra points at $s=-0.15$ and −0.10 bohr, respectively, were added to the ISPE calculation in order to reproduce more precisely the maximum of the high level energy profile. As it can be inferred from Table I, the maximum of the multilevel classical potential energy profile does not necessarily coincide with the saddle point location at the electronic level used for geometry optimization. For the MCSAC meth-

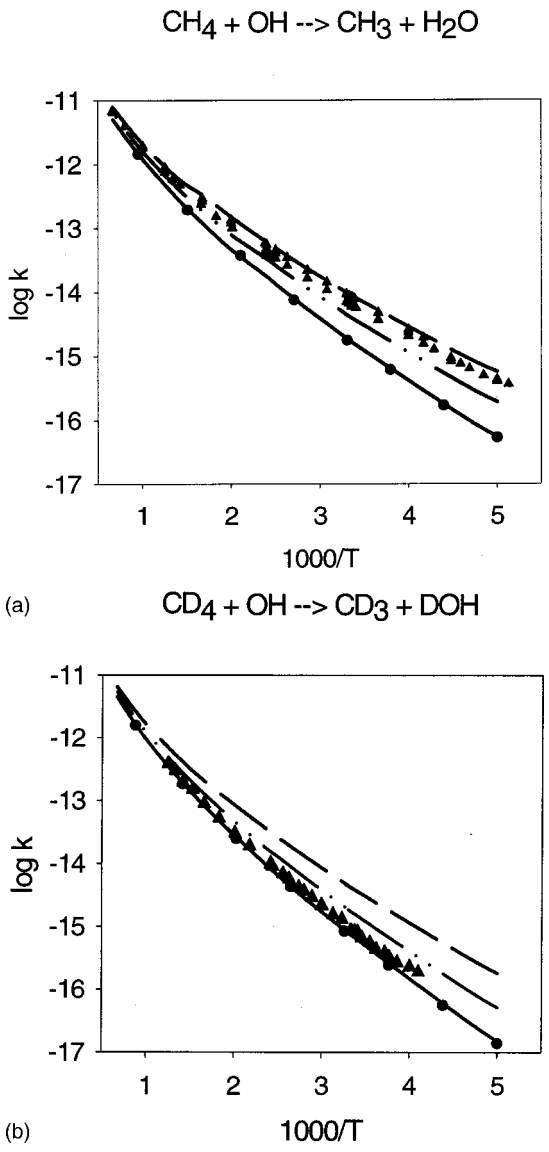

FIG. 1. Arrhenius plots for the experimental and calculated rate constants of (a) (R1); (b) (R5). Rate constants are in $cm^3\,molecule^{-1}\,s^{-1}$ and temperatures in Kelvin. Experimental data from Refs. 12–19 (triangles); MCSAC-CCSD(T)/cc-pVTZ-1*sc* (dashed–dashed line); MCSAC-CCSD(T)/cc-pVTZ-2*sc* (solid line); MCSAC-CCSD(T)/cc-pVTZ-2*s* (dashed–dotted–dotted line); MCSAC-CCSD(T)/cc-pVTZ-2*m* (dots). The MCSAC-CCSD(T)/cc-pVTZ-2*sc* and -2*m* methods give the same Arrhenius plots for (R1) and (R5).

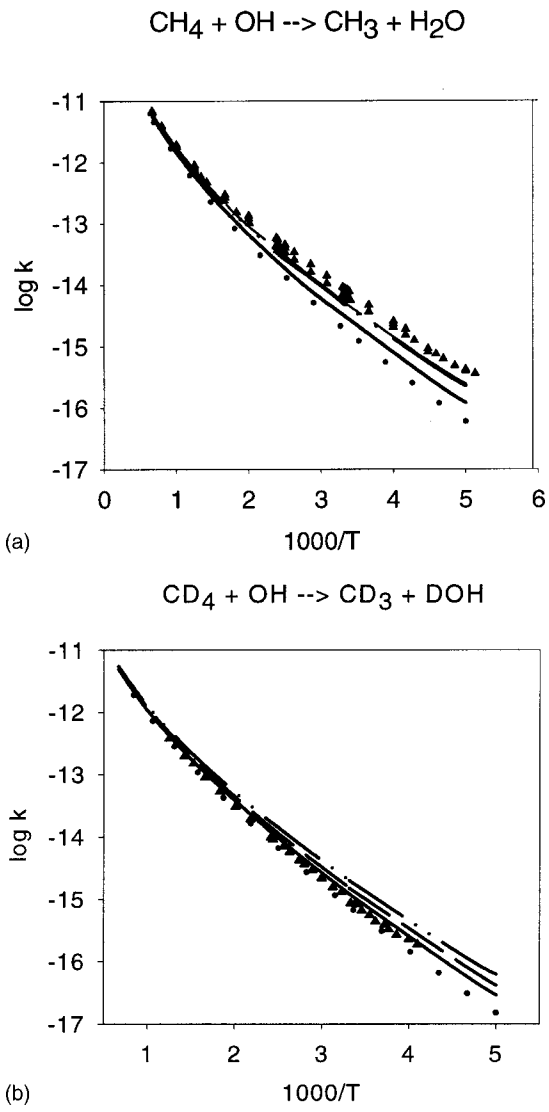

FIG. 2. Arrhenius plots for the experimental and calculated rate constants of (a) (R1); (b) (R5). Rate constants are in $cm^3\,molecule^{-1}\,s^{-1}$ and temperatures in Kelvin. Experimental data from Refs. 12–19 (triangles); MCCM-CCSD(T)-1*sc* (dashed–dashed line); MCCM-CCSD(T)-2*sc* (solid line); MCCM-CCSD(T)-2*s* (dashed–dotted–dotted line); MCCM-CCSD(T)-2*m* (dots). The MCCM-CCSD(T)-1*sc* and -2*s* methods give the same Arrhenius plots for (R1).

ods used in this work, the location of the multilevel maximum on the MP2(full)/cc-pVTZ MEP occurs at *s* values that go from -0.06 to -0.15 bohr, which represents an increase in the classical potential energy barrier ($V_{max}-V^{\neq}$) from 0.01 up to 0.16 kcal/mol. For the MCCM methods there is no significant displacement from the MP2(full)/cc-pVTZ saddle point. There is less dispersion in the MCCM-CCSD(T) classical energy barriers ($V_{max}=5.06-5.62$ kcal/mol) than in the MCSAC-CCSD(T)/cc-pVTZ ones ($V_{max}=4.20-5.53$ kcal/mol). This trend is also observable in the maximum values of the adiabatic energy profile, located between $-0.30>s>-0.34$ bohr for the MCSAC methods and at -0.29 or -0.30 bohr for the MCCM schemes.

All the values of V_{max} in Table I, except for the MCSAC-CCSD(T)/cc-pVTZ-1*sc* one, are close to the value of 5.11 kcal/mol (once corrected by -0.15 kcal/mol to account for spin–orbit effects) at the CBS-QCI/APNO//ML (that is, fully optimized at the CBS-QCI/APNO level) saddle point structure of Malick *et al.*[4] These authors state that when calculating dual-level or multilevel barrier heights, one should search for the Max{Method 1}//MEP{Method 2} to reduce the error of the low level saddle point geometry if the HL optimization is not available.

In Figs. 1 and 2, the Arrhenius plots for the MCSAC-CCSD(T)/cc-pVTZ and MCCM-CCSD(T) ISPE calculations, respectively, are depicted for (R1) (a) and (R5) (b). Also the available experimental rate constants are represented. It can be seen in Fig. 1 (see also Table I) that the two MCSAC methods with the highest adiabatic energy barrier (2*sc* and 2*m*) underestimate (R1) experimental rate con-

TABLE II. Maximum value of the classical energy profile (V_{max}), adiabatic energy barrier (ΔV_a^G), bond lengths of the structure at V_{max}, and classical reaction energy (ΔV). All energies in kcal/mol and distances in Å. See scheme 1 for numbering of nuclei.

Method of calculation	V_{max}	ΔV_a^G	$R(C_2-H_5)$	$R(H_5-O_6)$	ΔV
MP2(full)/6-31G(d)	14.0	12.2[a]	1.23	1.27	−7.6
QCISD(fc)/6-31G(d)	15.0	13.1[a]	1.27	1.23	−3.7
QCID(fc)/cc-pVDZ[b]	13.9	⋯	1.25	1.25	−6.4
QCISD(fc)/cc-pVDZ[b]	11.2	⋯	1.26	1.25	−6.5
MP2(full)/cc-pVTZ	8.4	7.0[a]	1.18	1.32	−15.0
QCISD/6-311G**[c]	11.1	⋯	1.24	1.25	−8.9[d]
QCISD(fc)/cc-pVTZ	9.5	7.9[a]	1.23	1.27	−10.3
CBS-RAD(Q,Q)//MEP{QCISD(fc)/6-31G(d)}	6.0	4.4[a]	1.12	1.41	−12.9
CBS-RAD(Q,Q)//MEP{MP2(full)/cc-pVTZ}	6.2	6.7	1.13	1.37	−14.8
MC-QCISD//MEP{MP2(full)/6-31G(d)}	7.5	8.3[a]	1.12	1.38	−15.5
MC-QCISD//MEP{MP2(full)/cc-pVTZ}	7.3	7.8	1.14	1.37	−15.5
MCSAC-CCSD(T)-2s//MEP{MP2(full)/cc-pVTZ}	4.9	5.5	1.14	1.37	−12.4
MCCM-CCSD(T)-1sc//MEP{MP2(full)/cc-pVTZ}	5.2	5.5	1.18	1.32	−12.8
CBS-QCI/APNO//MEP{QCISD/6-311G**}(−0.15)[c]	5.60	⋯	1.14	1.37	−13.5[d]
MCCM-CCSD(T)-1sc//QCISD(fc)/cc-pVTZ	4.9	4.6	1.23	1.27	−12.7
CBS-QCI/APNO//ML(−0.15)[c]	5.11	⋯	1.17	1.39	⋯
Expt.[e]	⋯	⋯	⋯	⋯	−13.5
Expt. reaction enthalpy at 298 K	⋯	⋯	⋯	⋯	−14.4

[a]Adiabatic energy at V_{max}.
[b]Taken from Ref. 8.
[c]Taken from Ref. 4.
[d]Reaction enthalpy at 298 K.
[e]Experimental reaction energy taken from Ref. 67.

stants for the whole range of temperatures, and the results for (R5) are also slightly underestimated at low temperatures. In the same way, the method with the lowest adiabatic energy barrier (1sc) fairly reproduces (R1) rate constants (although slightly overestimated below 600 K) and somewhat overestimates the rate constants for (R5). The MCSAC method that gives the best results (2s) has an adiabatic energy maximum of 5.50 kcal/mol. It slightly underestimates the results for (R1) below 700 K, and slightly overestimates (R5) rate constants in the available experimental data temperature range (244–800 K). At the MCCM-CCSD(T) level of theory (see Fig. 2 together with Table I), the 1sc and 2s methods give practically the same rate constants for (R1), in both cases slightly underestimated below 500 K when compared to experiment. For (R5), both methods overestimate the available experimental results, although the 1sc method gives significatively better results than the 2s method. The 2m method, that has the highest adiabatic energy barrier of the MCCM methods used in this work, and the 2sc method underestimate the (R1) rate constants but for (R5) they agree well to experimental data over a wide range of temperatures.

Therefore, as can be seen from these results, the challenge consists of reproducing both (R1) and (R5) experimental rate constants at the same electronic level. The best balanced of those results presented above are the MCSAC-CCSD(T)/cc-pVTZ-2s and the MCCM-CCSD(T)-1sc ISPE calculations, the later giving the most accurate rate constants over the whole available experimental data temperature range.

B. CBS-RAD and MC-QCISD calculations for (R1)

The CBS-RAD(Q,Q) (Ref. 38) multilevel single-point energy scheme is based on QCISD(fc)/6-31G(d) geometries. The exoergicity for (R1) at the QCISD(fc)/6-31G(d) level is highly underestimated (see Table II), and results in a saddle point structure with $R(C_2-H_5)=1.27$ Å and $R(O_6-H_5)=1.23$ Å (Scheme 1).

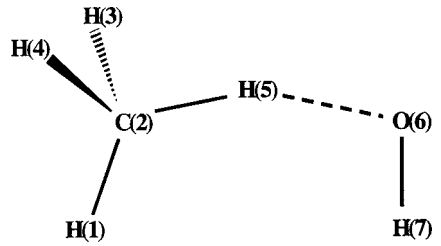

Scheme 1.

In contrast, the CBS-RAD(Q,Q) exoergicityvalue of −12.9 kcal/mol is similar to the MCCM values of Table I. As we have explained above, we have carried out an intermediate-IOC dual-level direct dynamics calculation using the MP2(full)/cc-pVTZ MEP from paper I as the LL, and the CBS-RAD(Q,Q) calculations at the stationary points as the HL. A value of 0.68 bohr, calculated from the LL MEP, was taken for the L parameter in the intermediate-IOC calculation [see Eq. (5b) of Ref. 35]. The results for (R1) rate constants are shown in Table III together with the experimental values of Atkinson[14] and Ravishankara and co-workers.[15,19] Although the HL CBS-RAD(Q,Q) classical energy barrier (4.8 kcal/mol) is within the values of Table I, the adiabatic energy barrier is only 4.3 kcal/mol as a consequence of the zero-point energy (ZPE) of the QCISD(fc)/6-31G(d) saddle point. This results in that the CBS-RAD(Q,Q) intermediate-IOC

TABLE III. Rate constants (in $cm^3\,molecule^{-1}\,s^{-1}$) at several temperatures (power of 10 in parentheses) for (R1), calculated at the CBS-RAD, MC-QCISD, and MCCM-CCSD(T)//QCISD(fc)/cc-pVTZ electronic levels.[a]

	$k_1^{CVT/SCT}$					
T (K)	CBS-RAD(Q,Q) intermediate-IOC	CBS-RAD//MP2(full)/cc-pVTZ ISPE	MC-QCISD intermediate-IOC	MC-QCISD//MP2(full)/cc-pVTZ ISPE	MCCM-CCSD(T)//QCISD(fc)/cc-pVTZ intermediate-IOC	k_1^{expt}
200	1.61(−15)	1.21(−17)	1.80(−17)	1.50(−18)	7.86(−16)	4.0±0.2(−16)[b]
223	3.66(−15)	3.66(−17)	5.48(−17)	5.27(−18)	1.80(−15)	8.2±4.2(−16)[b]
298	2.30(−14)	5.54(−16)	8.04(−16)	1.19(−16)	1.27(−14)	6.35(−15)[c]
300	2.39(−14)	5.87(−16)	8.52(−16)	1.27(−16)	1.32(−14)	6.62(−15)[c]
350	5.77(−14)	2.10(−15)	2.97(−15)	5.49(−16)	3.25(−14)	1.63(−14)[c]
400	1.16(−13)	5.80(−15)	7.97(−15)	1.76(−15)	6.62(−14)	3.38(−14)[c]
420	1.48(−13)	8.23(−15)	1.12(−14)	2.35(−15)	8.46(−14)	4.37(−14)[c]
500	3.35(−13)	2.34(−14)	3.50(−14)	8.83(−15)	1.94(−13)	1.34(−13)[d]
600	7.31(−13)	6.92(−14)	1.02(−13)	3.04(−14)	4.25(−13)	2.95(−13)[d]
700	1.35(−12)	1.59(−13)	2.13(−13)	7.80(−14)	7.86(−13)	···
1000	4.50(−12)	8.54(−13)	1.13(−12)	5.15(−13)	2.65(−12)	1.93(−12)[d]
1500	1.68(−11)	4.19(−12)	5.66(−12)	2.82(−12)	9.86(−12)	6.65(−12)[d]

[a]See Results and Discussion for more details.
[b]From Ref. 19.
[c]From Ref. 15.
[d]From Ref. 14.

rate constant at 200 K is overestimated by a factor of 4.0, and at 1500 K it is still 2.5 times higher than the experimental one.

At this point, some considerations have to be done. The geometry bond lengths given in columns 4 and 5 of Table II show that the location of the saddle point structure is very dependent on the level of the optimization, as it has already been observed in several other works. Generally, the more exoergic the reaction is, the more reactantlike the saddle point structure looks like, in accordance to Hammond's postulate (compare the seven first rows of Table II that resume the single-level results). The geometry discrepancy between the highest single-level optimized structure calculated in this work [at the QCISD(fc)/cc-pVTZ level] and the CBS-QCI/APNO//ML structure of Malick *et al.*[4] is probably related to the underestimated exoergicity given by the QCISD(fc)/cc-pVTZ method (−10.3 kcal/mol). For the same reason an even greater difference is found between the QCISD(fc)/6-31G(d) saddle point structure and the CBS-QCI/APNO//ML saddle point. Malick *et al.*[4] have demonstrated that the CBS-QCI/APNO//ML saddle point structure is closer to the Max{CBS-QCI/APNO}//MEP{QCISD/6-311G**} geometry than to the QCISD/6-311G** saddle point (compare geometry bond lengths in rows six, fourteen, and sixteen of Table II). Therefore, it was reasonable to assume that the CBS-RAD(Q,Q)//ML saddle point structure would also be closer to the Max{CBS-RAD(Q,Q)}//MEP{QCISD(fc)/6-31G(d)} geometry than to the QCISD(fc)/6-31G(d) saddle point. Consequently, we then searched for the Max{CBS-RAD(Q,Q)}//MEP{QCISD(fc)/6-31$G(d)$} structure. As it can be seen in Table II, this maximum moves to reactants [R(C–H)=1.12 Å and R(O–H)=1.41 Å] and the classical barrier height increases by 1.2 kcal/mol compared to the HL CBS-RAD(Q,Q) values calculated at the LL saddle point structure. However, the generalized vibrational mode analysis at this structure of maximum classical energy gives three imaginary frequencies whatever coordinates, Cartesian or redundant internal, are used and although the MEP was calculated with the *tight* criteria of the GAUSSIAN 94 package and we have applied the RODS algorithm in the normal mode analysis. These imaginary frequencies do not seem to have any physical meaning like existence of ''ridges'' or branching points on the PES. On the contrary, they probably are a consequence of numerical errors resulting from a poor description of the PES and the generalized vibrational modes at the QCISD(fc)/6-31G(d) level, at least in this region away from the saddle point structure (around $s=-0.33$ bohr).

In order to account for the displacement of the HL saddle point structure with respect to the LL saddle point, an ISPE calculation could be an appropriate approach for the dynamical study of (R1) at the CBS-RAD(Q,Q) electronic level. However, we have already commented on the difficulties to obtain reliable generalized vibrational frequencies along the QCISD(fc)/6-31G(d) MEP. At this point, we decided to carry out a CBS-RAD//MP2(full)/cc-pVTZ ISPE calculation, that is, using as the LL the MP2/(full)/cc-pVTZ MEP instead of the QCISD(fc)/6-31G(d) MEP. As it can be seen in Table II, the reaction exoergicity is overestimated in this scheme by 1.3 kcal/mol, when compared to the experimental value. An extra point at $s=-0.12$ bohr was added to the five above mentioned in order to reproduce the classical energy maximum in the ISPE calculation. This maximum of the HL classical energy profile is higher (0.2 kcal/mol) than the Max{CBS-RAD(Q,Q)}//MEP{QCISD(fc)/6-31G(d)} value. The calculated rate constants for (R1) are listed in Table III. They are lower than all the MCSAC and MCCM results, and lower than the experimental ones (more than one order of magnitude at 200 K, compared to the MCCM results and to experiment, and around 1.4 times or 1.6 times at 1500 K, compared to the MCCM results and to experiment, respectively).

The MC-QCISD multilevel energy calculations at the MP2(full)/6-31G(d) stationary point structures give an exo-

ergicity for (R1) overestimated by 2 kcal/mol when compared to experiment (see Table II) and a classical energy barrier of 6.7 kcal/mol, which is more than 1 kcal/mol higher than the MCSAC and the MCCM values of Table I. Hence, it seems that the MC-QCISD method may not correct the tendency of MP2 calculations on hydrogen abstraction reactions to give overestimated classical barrier heights and, when used with large basis sets, to overestimate reaction exoergicities. We then carried out an intermediate-IOC dual-level direct dynamics calculation using the MP2(full)/cc-pVTZ MEP from paper I as the LL, and the MC-QCISD calculations at the stationary points as the HL. The results for the intermediate-IOC (R1) rate constants using the MC-QCISD multilevel scheme are shown in Table III. In accordance with the high classical energy value commented above and the high adiabatic energy barrier (6.7 kcal/mol), the MC-QCISD intermediate-IOC rate constants underestimate the experimental values over the whole range of temperatures, by a factor of 22 at 200 K and a factor of 1.17 at 1500 K. We then searched for the Max{MC-QCISD}//MEP{MP2(full)/6-31G(d)} structure (see Table II). This structure at V_{max} is more reactantlike [$R(C_2-H_5)=1.12$ Å and $R(O_6-H_5)=1.38$ Å] than the MP2(full)/6-31G(d) saddle point and its classical energy barrier increases up to 7.5 kcal/mol. Comparing this Max{MC-QCISD}//MEP{MP2(full)/6-31G(d)} and the Max{MC-QCISD}//MEP{MP2(full)/cc-pVTZ} energies in Table II, it seems that the MP2(full)/cc-pVTZ MEP could be as appropriate for the MC-QCISD multilevel calculations of (R1) as the MP2(full)/6-31G(d) MEP. Therefore, we carried out the dual-level direct dynamics ISPE calculation by using the MP2(full)/cc-pVTZ MEP as the LL and the MC-QCISD classical energies as the HL information. As could be expected from the high classical energy barrier (7.3 kcal/mol) and the still higher adiabatic energy barrier (7.8 kcal/mol) the MC-QCISD//MP2(full)/cc-pVTZ rate constants in Table III are underestimated over the whole range of temperatures (more than two orders of magnitude at 200 K and 2.4 times at 1500 K) when compared to the experimental results.

Truhlar and co-workers[20(b)] pointed out that the main disadvantage of the ISPE scheme as compared to the strictly IOC scheme (that is, the method that interpolates corrections to a LL PES by carrying out the optimization of the stationary points structures, the calculation of their frequencies and of their classical energies at the same HL) is that in the ISPE procedure the HL energies are single-point calculations along a lower level reaction path that may differ from the higher level reaction path. This means that if one searches for the maximum higher level energy along the lower level path, the result will be systematically too high and it will be dependent on the LL used for geometry optimization. The same authors consider that there is no advantage then in following the procedure of finding the Max{HL}//MEP{LL} as compared to just evaluating HL//LL at the lower level saddle point. Moreover, if the lower level geometry for the saddle point is incorrect, the barrier height predicted by electronic structure calculations based upon this geometry is most likely incorrect as well. For that reason, Truhlar and co-workers[20(b)] originally recommended using geometry optimization at the higher level within an IOC dual-level direct dynamics scheme. As can be seen in Table II, it is not clear which is the best method to calculate the geometries for the entitled reactions, and it also depends on the HL used. Nevertheless, as it can be inferred from Table I of paper I together with Table II of the present work, the high single-level electronic structure method one should use in the IOC scheme to obtain the accurate thermodynamics and rate constants, at least for hydrogen abstraction reactions, is nowadays computationally unaffordable. The two alternative approaches are then: an intermediate-IOC calculation using the highest affordable single-level of optimization and frequency calculation or an actual IOC calculation using a multilevel classical energy and geometry optimization, like the CBS-QCI/APNO//ML numerical calculation of Malick *et al.*,[4] but including, in addition, the evaluation of second derivatives of the multilevel energy expression.

C. MCCM-CCSD(T)//QCISD(fc)/cc-pVTZ calculations for (R1)

In this work, dual-level direct dynamics calculations using the intermediate-IOC approach but carrying out the optimization and second derivatives calculation at as high level as possible are also included. In this intermediate scheme the LL information consisted in the MP2(full)/cc-pVTZ MEP but it was corrected from the following HL information at the stationary points: classical energies calculated at the MCCM-CCSD(T) level, geometries and frequencies obtained at the QCISD(fc)/cc-pVTZ level. The MCCM-CCSD(T)//QCISD(fc)/cc-pVTZ reaction energy and classical energy barrier height, given in Table II, differ by only 0.06–0.18 kcal/mol and 0.16–0.72 kcal/mol, respectively, from the values obtained with the MCCM multilevel classical energies at the MP2(full)/cc-pVTZ geometries (see Table I). Truhlar and co-workers[8] recently proposed the use of UQCISD, UQCISD(T), UCCSD, and UCCSD(T) methods for geometry optimization of the open-shell transition states for radical reactions. The QCISD(fc)/cc-pVTZ saddle point geometry (see Table II) of the perprotio reaction is less reactantlike than the MP2(full)/cc-pVTZ saddle point but slightly more reactantlike than the QCISD(fc)/cc-pVDZ structure. It is interesting to remark the agreement between the UCCD(fc)/cc-pVTZ saddle point geometry for (R1) of Truhlar and co-workers[8] and the optimized structure for the QCISD(fc)/cc-pVTZ saddle point. This fact confirms that UCCD geometries are very similar to UQCISD ones for (R1). When zero point energy effects are corrected using the QCISD(fc)/cc-pVTZ frequencies at the stationary points, the MCCM-CCSD(T)//QCISD(fc)/cc-pVTZ adiabatic energy barrier (located at $s=-0.29$ bohr) has a value of 4.6 kcal/mol. This energy barrier is 0.76 kcal/mol to 1.4 kcal/mol lower than the MCCM-CCSD(T)/cc-pVTZ adiabatic barriers shown in Table I. The MCCM-CCSD(T)//QCISD(fc)/cc-pVTZ intermediate-IOC rate constant values are given in Table III. These results show a good agreement with experimental rate constants over the whole temperature range, slightly overestimating the experimental rate constants (for instance, at 200 K by a factor of 1.96 and by a factor of 1.48 at 1500 K).

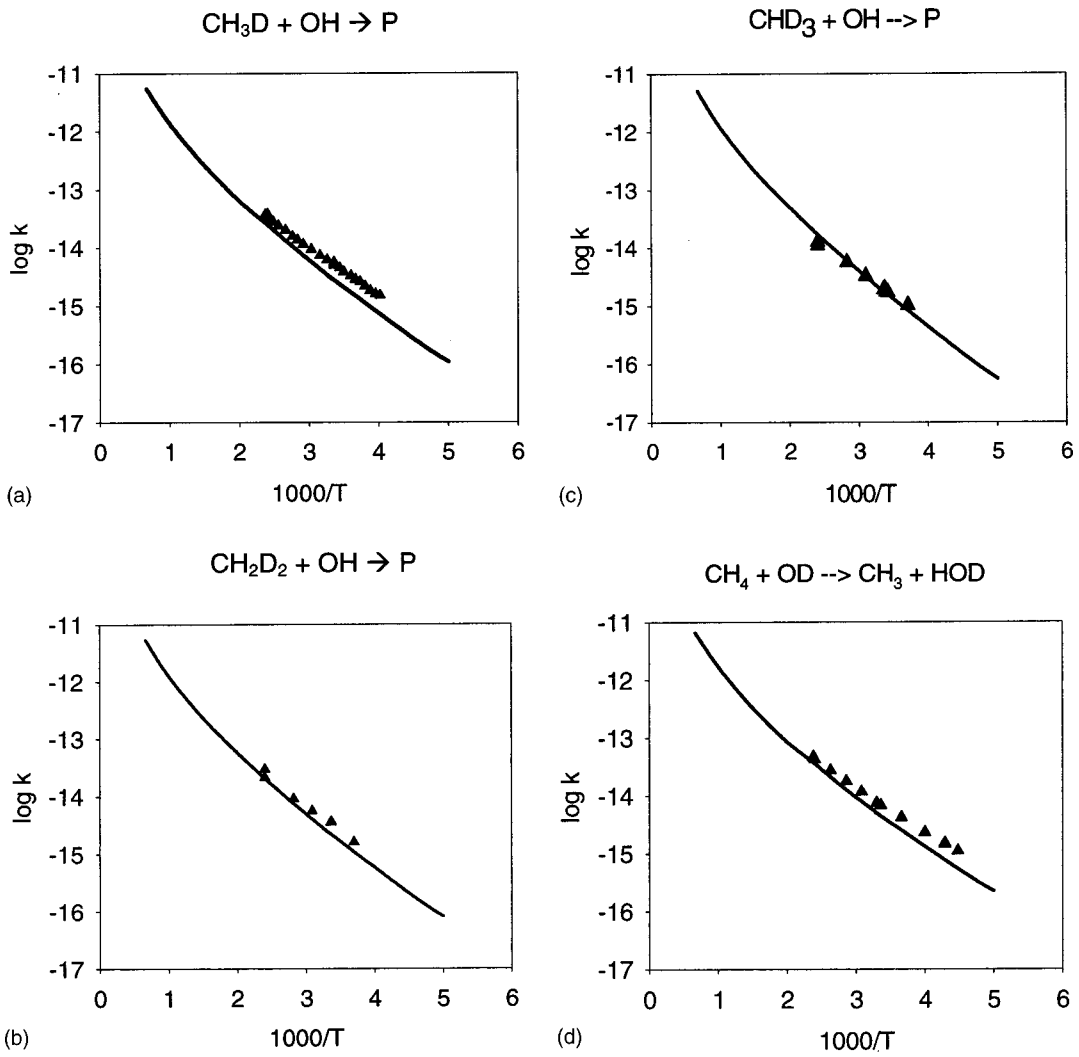

FIG. 3. Arrhenius plots for the experimental (Ref. 19) and MCCM-CCSD(T)-1*sc* calculated rate constants of (a) (R2); (b) (R3); (c) (R4); (d) (R6). Rate constants are in cm^3 $molecule^{-1}$ s^{-1} and temperatures in Kelvin. Experimental data (triangles); calculated rate constants (solid lines).

D. Rate constant calculations for (R2), (R3) (R4), and (R6) reactions

The method used in this work that best reproduces both (R1) and (R5) experimental rate constants is the MCCM-CCSD(T)-1*sc* multilevel scheme. Hence, the rate constants for the reactions (R2)–(R4) and (R6) were calculated with a MCCM-CCSD(T)-1sc ISPE direct dynamics calculation. The resulting Arrhenius plots are depicted in Fig. 3. It can be seen from these graphs that the calculated rate constants agree better with the experimental results as the isotopic substitution is augmented. As in paper I, this is a consequence of the fact that the calculated rate constants for

TABLE IV. Rate constants (in cm^3 $molecule^{-1}$ s^{-1}) at several temperatures (power of 10 in parentheses) for (R1)–(R6) using the VTST-ISPE algorithm at the MCCM-CCSD(T)-1*sc* level.

T (K)	(R1)	(R2)	(R3)	(R4)	(R5)	(R6)
200	1.51(−16)	1.10(−16)	8.18(−17)	5.62(−17)	4.13(−17)	2.25(−16)
223	3.74(−16)	2.81(−16)	2.16(−16)	1.56(−16)	1.19(−16)	5.33(−16)
298	3.45(−15)	2.76(−15)	2.22(−15)	1.75(−15)	1.45(−15)	4.45(−15)
300	3.61(−15)	2.89(−15)	2.34(−15)	1.84(−15)	1.53(−15)	4.66(−15)
350	1.03(−14)	8.40(−15)	6.84(−15)	5.58(−15)	4.61(−15)	1.27(−14)
400	2.36(−14)	1.96(−14)	1.61(−14)	1.34(−14)	1.14(−14)	2.85(−14)
420	3.14(−14)	2.63(−14)	2.17(−14)	1.81(−14)	1.56(−14)	3.77(−14)
500	7.31(−14)	6.34(−14)	5.74(−14)	5.04(−14)	4.43(−14)	8.50(−14)
600	1.80(−13)	1.59(−13)	1.42(−13)	1.26(−13)	1.18(−13)	2.06(−13)
700	3.63(−13)	3.25(−13)	2.89(−13)	2.63(−13)	2.52(−13)	4.09(−13)
1000	1.53(−12)	1.39(−12)	1.26(−12)	1.19(−12)	1.18(−12)	1.70(−12)
1500	5.87(−12)	5.51(−12)	5.28(−12)	5.13(−12)	5.24(−12)	6.58(−12)

(R1) and (R5) are slightly underestimated and overestimated, respectively, giving compensated results for (R2)–(R4). For (R2), the rate constants are lower than the experimental results at all the temperatures studied (especially at low temperatures). For (R3), they are only underestimated below 400 K, and for (R4) the agreement with the experimental results is good at all the available temperature data. Finally, the calculated rate constants for (R6) are slightly underestimated, specially at low temperatures.

In Table IV, the results for (R1)–(R6) are presented. Although rather small for (R3)–(R6), all the rates k_1/k_i [where i stands for (R2)–(R6)] reproduce the experimental tendency.

IV. CONCLUSIONS

In a previous paper we theoretically calculated the rate constants and their temperature dependence for the reactions $CH_nD_{4-n}+OH \rightarrow P$, and for the reaction of methane with OD, by means of variational transition state theory plus multidimensional corrections at several very high electronic levels. The results were quite good although the available experimental rate constants were not matched exactly. In the present work we have repeated those calculations using different multilevel electronic methods including two very recently developed multicoefficient schemes for extrapolating correlated electronic structure calculations (MCSAC and MCCM).

We have shown that the so-called MCCM-CCSD(T)-1*sc* multilevel scheme provides the best results for the set of reactions studied. The calculated rate constants turn out to be in general somewhat better than the ones we have previously found. However, a slight difference from the experimental rate constants still persists, specially at the lowest temperatures. Anyway, we think that the best theoretical rate constants of the present paper are already accurate enough for most of the practical applications what validates the efficiency of the multilevel multicoefficient schemes. We have to underline that no fitting to the experimental data (beyond the ones implicit in the multicoefficient schemes) has been performed along this paper. Interestingly, some kinetic isotope effects (KIEs) are not so well reproduced. It is generally assumed that the errors in the rate constants of the different isotopomers cancel when the KIEs are calculated. However, this is true when the deviations of the individual theoretical rate constants from the experimental ones go in the same direction. This is not the case here. The MCCM-CCSD(T)-1*sc* multilevel scheme slightly underestimates the CH_4+OH reaction but slightly overestimates the CD_4+OH reaction. As a consequence, both errors, although being very small, reinforce when the corresponding KIE is calculated. The opposite behavior of the CH_4 and CD_4 theoretical results versus the corresponding experimental ones could be better attributed to factors related with the shape of the adiabatic potential energy profile, which depends on the frequencies and highly influence on the tunneling transmission factors. On the other hand, it has to be pointed out that the SCT semiclassical adiabatic ground-state approximation has been used to correct for tunneling in this work. The lack of use of a large-curvature tunneling (LCT) approach could be an additional source of error. Additional theoretical work on these reactions trying to improve the calculated KIEs is now in progress in our laboratory.

[1] K. D. Dobbs, D. A. Dixon, and A. Komornicki, J. Chem. Phys. **98**, 8852 (1993).
[2] H. Basch and S. Hoz, J. Phys. Chem. A **101**, 4416 (1997).
[3] M. Schwartz, P. Marshall, R. J. Berry, C. J. Ehlers, and G. A. Petersson, J. Phys. Chem. A **102**, 10074 (1998).
[4] D. K. Malick, G. A. Petersson, and J. A. Montgomery, Jr., J. Chem. Phys. **108**, 5704 (1998).
[5] F. A. Hamprecht, A. J. Cohen, D. J. Tozer, and N. C. Handy, J. Chem. Phys. **109**, 6264 (1998).
[6] J. Korchowiec, S. Kawahara, K. Matsumura, T. Uchimaru, and M. Sugie, J. Phys. Chem. A **103**, 3548 (1999).
[7] M. Sodupe, J. Bertrán, L. Rodríguez-Santiago, and E. J. Baerends, J. Phys. Chem. A **103**, 166 (1999).
[8] Y.-Y. Chuang, E. L. Coitiño, and D. G. Truhlar, J. Phys. Chem. A **104**, 446 (2000).
[9] L. Masgrau, A. González-Lafont, and J. M. Lluch, J. Chem. Phys. **114**, 2154 (2001).
[10] D. G. Truhlar, A. D. Isaacson, and B. C. Garrett, in *Theory of Chemical Reaction Dynamics*, edited by M. Baer (CRC, Boca Raton, 1985), Vol. IV, p. 65.
[11] S. C. Tucker and D. G. Truhlar, in *New Theoretical Concepts for Understanding Organic Reactions*, edited by J. Bertrán and I. G. Csizmadia (Kluwer Academic, Dordrecht, 1989), p. 291.
[12] S. Gordon and W. A. Mulac, Int. J. Chem. Kinet. **1**, 289 (1975).
[13] D. L. Baulch, M. Bowers, D. G. Malcom, and R. T. Tuckerman, J. Phys. Chem. Ref. Data **15**, 465 (1986), and references therein.
[14] R. Atkinson, J. Phys. Chem. Ref. Data **1**, 18 (1989).
[15] G. L. Vaghjiani and A. R. Ravishankara, Nature (London) **350**, 406 (1991).
[16] J. R. Dunlop and F. P. Tully, J. Phys. Chem. **97**, 11148 (1993).
[17] W. B. DeMore, J. Phys. Chem. **97**, 8564 (1993).
[18] W. B. DeMore, S. P. Sander, D. M. Golden, R. F. Hampson, M. J. Kurylo, C. J. Howard, A. R. Ravishankara, C. E. Kolb, and M. J. Molina, "Chemical kinetics and photochemical data for use in stratospheric modeling," Evaluation number 12, jpl Publication 97–4, Jet Propulsion Laboratory, California Institute of Technology, Pasadena, CA, 1997.
[19] T. Gierczak, R. K. Talukdar, S. C. Herndon, G. L. Vaghjiani, and A. R. Ravishankara, J. Phys. Chem. A **101**, 3125 (1997).
[20] (a) W. T. Duncan, R. L. Bell, and T. N. Truong, J. Comput. Chem. **19**, 1039 (1998); (b) Y.-Y. Chuang, J. C. Corchado, and D. G. Truhlar, J. Phys. Chem. A **103**, 1140 (1999).
[21] M. S. Gordon and D. G. Truhlar, J. Am. Chem. Soc. **108**, 5412 (1986).
[22] I. Rossi and D. G. Truhlar, Chem. Phys. Lett. **234**, 64 (1995).
[23] P. L. Fast, J. C. Corchado, M. L. Sánchez, and D. G. Truhlar, J. Phys. Chem. A **103**, 3139 (1999).
[24] G. A. Petersson, ACS Symp. Ser. **677**, 237 (1998).
[25] J. M. L. Martin, ACS Symp. Ser. **677**, 212 (1998).
[26] M. R. A. Blomberg and P. E. M. Siegbahn, ACS Symp. Ser. **677**, 197 (1998).
[27] J. C. Corchado and D. G. Truhlar, ACS Symp. Ser. **712**, 106 (1998).
[28] D. G. Truhlar, Chem. Phys. Lett. **294**, 45 (1998).
[29] Y.-Y. Chuang and D. G. Truhlar, J. Phys. Chem. A **103**, 651 (1999).
[30] P. L. Fast, M. L. Sánchez, and D. G. Truhlar, J. Chem. Phys. **111**, 2921 (1999).
[31] C. M. Tratz, P. L. Fast, and D. G. Truhlar, Phys. Chem. Commun. **2**, article 14, 1–10 (1999).
[32] P. L. Fast, J. C. Corchado, M. L. Sánchez, and D. G. Truhlar, J. Phys. Chem. A **103**, 5129 (1999).
[33] P. L. Fast, M. L. Sánchez, J. C. Corchado, and D. G. Truhlar, J. Chem. Phys. **110**, 11679 (1999).
[34] P. L. Fast, M. L. Sánchez, and D. G. Truhlar, Chem. Phys. Lett. **306**, 407 (1999).
[35] W.-P. Hu, Y.-P. Liu, and D. G. Truhlar, J. Chem. Soc., Faraday Trans. **90**, 1715 (1994).
[36] Y.-Y. Chuang and D. G. Truhlar, J. Phys. Chem. A **101**, 3808 (1997).
[37] P. L. Fast and D. G. Truhlar, J. Phys. Chem. A **104**, 6111 (2000).
[38] P. M. Mayer, C. J. Parkinson, and L. Radom, J. Chem. Phys. **108**, 604 (1998).
[39] J. W. Ochterski, G. A. Petersson, and J. A. Montgomery, Jr., J. Chem. Phys. **104**, 2598 (1996).

[40] W. J. Hehre, L. Radom, P. v. R. Schleyer, and J. A. Pople, in *Ab Initio Molecular Orbital Theory* (Wiley, New York, 1986).
[41] C. Møller and M. S. Plesset, Phys. Rev. **46**, 618 (1934).
[42] T. H. Dunning, Jr., J. Chem. Phys. **90**, 1007 (1989).
[43] K. Raghavachari, G. W. Trucks, J. A. Pople, and M. Head-Gordon, Chem. Phys. Lett. **157**, 479 (1989).
[44] P. L. Fast and D. G. Truhlar, J. Phys. Chem. A **103**, 3802 (1999).
[45] A. P. Scott and L. Radom, J. Phys. Chem. **100**, 16502 (1996).
[46] W. J. Hehre, R. Ditchfield, and J. A. Pople, J. Chem. Phys. **56**, 2257 (1972).
[47] L. A. Curtiss, K. Raghavachari, G. W. Trucks, and J. A. Pople, J. Chem. Phys. **109**, 7764 (1998).
[48] L. A. Curtiss, P. C. Redfern, K. Raghavachari, V. Rassolov, and J. A. Pople, J. Chem. Phys. **110**, 4703 (1999).
[49] J. A. Pople, M. Head-Gordon, and K. Raghavachari, J. Chem. Phys. **87**, 5968 (1987).
[50] (a) D. G. Truhlar and A. Kupperman, J. Am. Chem. Soc. **93**, 1840 (1971); (b) K. Fukui, Pure Appl. Chem. **54**, 1825 (1982).
[51] A. D. Isaacson and D. G. Truhlar, J. Chem. Phys. **76**, 1380 (1982).
[52] J. M. Rodgers, B. J. Lynch, P. L. Fast, Y.-Y. Chuang, J. Pu, and D. G. Truhlar, MULTILEVEL version 2.1, University of Minnesota, Minneapolis, 2000. http://comp.chem.umn.edu/multilevel
[53] M. J. Frisch, G. W. Trucks, H. B. Schlegel *et al.*, GAUSSIAN 94 (Gaussian, Inc., Pittsburgh, 1995).
[54] B. C. Garrett and D. G. Truhlar, J. Chem. Phys. **70**, 1593 (1979).
[55] B. C. Garrett and D. G. Truhlar, J. Phys. Chem. **83**, 1079 (1979).
[56] B. C. Garrett, D. G. Truhlar, R. S. Grev, and A. W. Magnuson, J. Phys. Chem. **84**, 1730 (1980).
[57] B. C. Garrett and D. G. Truhlar, J. Am. Chem. Soc. **101**, 4534 (1979).
[58] B. C. Garrett and D. G. Truhlar, J. Am. Chem. Soc. **101**, 5207 (1979).
[59] Y.-P. Liu, G. C. Lynch, T. N. Truong, D.-H. Lu, D. G. Truhlar, and B. C. Garrett, J. Am. Chem. Soc. **115**, 2408 (1993).
[60] P. Pechukas, J. Chem. Phys. **64**, 1516 (1976).
[61] J. Villà and D. G. Truhlar, Chem. Theor. Acc. **97**, 317 (1997).
[62] Y.-Y. Chuang and D. G. Truhlar, J. Phys. Chem. A **102**, 242 (1998).
[63] Y.-Y. Chuang and D. G. Truhlar, J. Chem. Phys. **112**, 1221 (2000).
[64] J. M. Rodgers, P. L. Fast, and D. G. Truhlar, J. Chem. Phys. **112**, 3141 (2000).
[65] J. C. Corchado, Y.-Y. Chuang, P. L. Fast *et al.*, POLYRATE 8.5.1, University of Minnesota, Minneapolis, 2000. http://comp.chem.umn.edu/polyrate
[66] W.-P. Hu and D. G. Truhlar, J. Am. Chem. Soc. **118**, 860 (1996).
[67] B. J. Lynch, P. L. Fast, M. Harris, and D. G. Truhlar, J. Phys. Chem. A **104**, 4811 (2000).

Theor Chem Acc (2002)
DOI 10.1007/s00214-002-0357-7

Theoretical
Chemistry Accounts

Regular article

Test of variational transition state theory with multidimensional tunneling contributions against experimental kinetic isotope effects for the CH_nD_{4-n} + OH→P (n = 0, 4) reactions

Laura Masgrau, Àngels González-Lafont, José M. Lluch

Departament de Química, Universitat Autònoma de Barcelona, 08193 Bellaterra, Barcelona, Spain

Received: 24 March 2002 / Accepted: 11 April 2002 / Published online: 4 July 2002

Abstract. Variational transition state theory including tunneling corrections (as implemented in Polyrate 8.7) and using multilevel energy calculations at the MCCM-CCSD(T)-1sc level for the CH_4 + OH reaction and at the MCCM-CCSD(T)-2m level for the CD_4 + OH process, reproduces very well the experimental rate constants. However, no single methodology was found that reproduces equally well the experimental rate constants for both title reactions.

Key words: Kinetic isotope effects – Multicoefficient correlation methods – Variational transition state theory rate constants – Reoriented dividing surface algorithm – CH_4 + OH reaction

The rate constants for the reaction of OH with methane and for several of its H/D isotopic variants have been the object of several experimental measurements [1] and theoretical calculations in the past [2]. The reactions of OH with methane and partially halogenated alkanes are especially important for controlling the balance of species in the upper atmosphere. In addition, the theoretical computation of accurate rate constants for the reaction of OH with methane and each of its deutero-isotopomers, has been, and still is, a challenge for electronic structure methods and dynamical approaches. One dynamical scheme that has been widely tested [3] against benchmark rate constants is variational transition state theory with multidimensional tunneling contributions (VTST/MT) [4]. However, the VTST/MT rate constants published in the literature for the title reactions, obtained with different levels of electronic structure calculations, do not match exactly the available experimental rate constants even though the results were quite good from a quantitative point of view (Melissas and Truhlar (1993), Hu et al. (1994), Espinosa-García and Corchado (2000), and Masgrau et al. (2001) [2]). In the last of these papers, we carried out a test of variational transition state theory plus multidimensional tunneling corrections using different multilevel electronic approaches. In particular, we used several of the MCSAC (multicoefficient scaling all correlation energy) and the MCCM (multicoefficient correlation methods) [5]. The so-called MCCM-CCSD(T)-1sc multilevel scheme provided the rate constants most comparable with the experimental ones for the reactions of OH with CH_4 and CD_4. Those results were good enough for most practical applications in the whole range of temperatures studied (especially for the perprotio reaction), although the deviation from experiment was larger at lower temperatures. Interestingly, the kinetic isotope effects (KIEs) were not so well reproduced because the deviations from the experimental values of the individual theoretical rate constants of the two different isotopologs, although being very small, are in opposite directions. The version of VTST/MT that we tested was CVT/SCT, in which CVT [6] stands for canonical variational theory and SCT [7] means the small curvature tunneling approximation. The MCCM-CCSD(T)-1sc multilevel electronic energy calculations mentioned above were used within a dual-level direct dynamics scheme known as the interpolated single-point energy correction (ISPE) [8]. This dual-level direct dynamics approach consisted in calculating a low-level MP2(full)/cc-pVTZ minimum energy path (MEP), with scaled generalized-normal-mode vibrational frequencies (with a scale factor of 0.9790) computed at the same level for selected points along this path. Then, multilevel single-point classical energy calculations were carried out at the stationary points and at several non-stationary points along the MEP as the high-level electronic information to correct the energetics. In addition, the reoriented dividing surface (RODS) algorithm [9] was applied to improve the generalized-normal-mode frequencies along the low-level MEP. Those calculations were carried out with POLYRATE version 8.5.1 [10].

Very recently, an improved version of the code was released. In particular, the modification affects the reaction path curvature vector calculation in the SCT

Correspondence to: À. González-Lafont
e-mail: angels@klingon.uab.es

methodology when the RODS algorithm is used. The question arises of whether that change could ameliorate the description of the KIEs. So, in this letter the KIEs corresponding to the reactions: CH_4/CD_4 + OH $\rightarrow$ H_2O/HDO + CH_3/CD_3 have been computed again with the improved RODS and SCT algorithms in POLYRATE 8.7 [11]. The three multilevel methods that will be tested are the MCCM-CCSD(T)-1sc, the MCCM-CCSD(T)-2sc and the MCCM-CCSD(T)-2m, and the dual-level direct dynamics approach will be the same as in our previous paper (last Ref. in [2]). The notation 1sc, 2sc, and 2m refers to the way in which the core-correlation and spin-orbit contributions are introduced and to the molecular data set used in the parametrization of the method.

In Fig. 1a the CVT/SCT rate constants for the CH_4 + OH reaction obtained with each one of the three selected direct dynamics methodologies are plotted, along with the experimental values, with respect to temperature. All the theoretical rate constants are improved in comparison with our previous calculations (last Ref. in [2]), especially in the lowest temperature range where tunneling is most significant, and where the improvement in the SCT algorithm in the new version of the code is expected to be more relevant. In the new calculations, the dynamical approach that gives the smallest average absolute deviation (19%) between the CVT/SCT rate constants and the experimental values, over the whole analyzed temperature range, is again the direct dynamics methodology based on the classical energy calculation at the MCCM-CCSD(T)-1sc level (note that the deviation is only of 3% between 298 °K and 420 °K). The CVT/SCT rate constants at the MCCM-CCSD(T)-2sc level are only slightly smaller (mean absolute deviation of 23%) although their behavior is better at the two lowest temperatures. These deviations are comparable to the average absolute deviation of 25% attributed to the intrinsic error of variational transition state theory with optimized multidimensional tunneling contributions (VTST/OMT) by a recent systematic comparison (by Allison and Truhlar [3]) of harmonic VTST/μOMT to 231 benchmark rate constants for colinear and three-dimensional atom-diatom reactions. At the MCCM-CCSD(T)-2m level the CVT/SCT rate constants slightly underestimate the experimental results and show greater deviations from experiment than the other two dynamical calculations. In Fig. 1b the rate constants calculated for the CD_4 + OH reaction with the three multilevel approaches are plotted along with experimental values as a function of temperature. The dynamical methodology based on corrected energies at the MCCM-CCSD(T)-2m level shows now a very small absolute average deviation, of only 10% from 298 °K to 700 °K, for this isotope variant of the perprotio reaction. However, the two other dynamical approaches based on multilevel classical energies at the MCCM-CCSD(T)-1sc and the MCCM-CCSD(T)-2sc levels overestimate the experimental rate constants, especially in the lowest temperature range, in contrast to the high accuracy attained for the CH_4 + OH reaction. In summary, none of these three dynamical approximations presents the same accuracy in the calculation of the rate constants for the CH_4 + OH and the

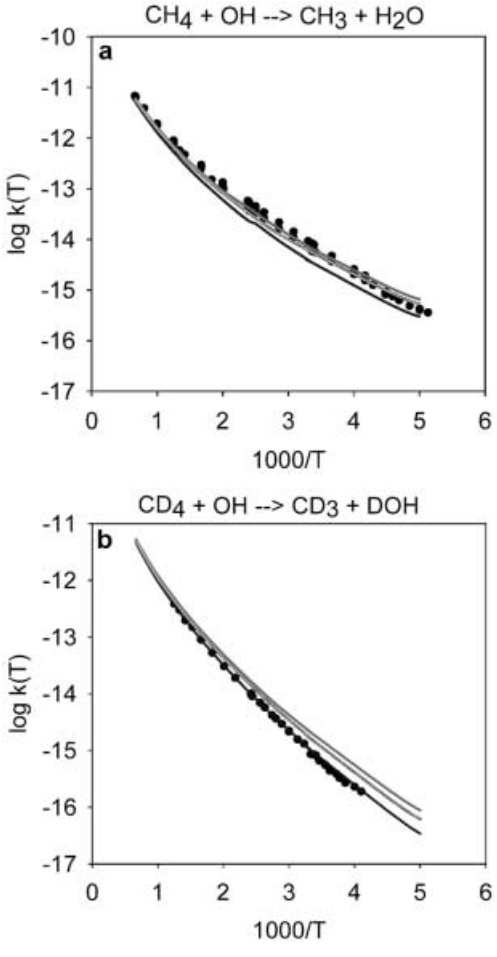

Fig. 1a, b. Arrhenius plots for the experimental and calculated rate constants of the reactions: **a** CH_4 + OH$\rightarrow$$CH_3$ + H_2O; **b** CD_4 + OH$\rightarrow$$CD_3$ + DOH. Rate constants are in cm^3 $molecule^{-1}$ s^{-1} and temperatures in Kelvin. Experimental data from Ref. [1] (*circles*); MCCM-CCSD(T)-1sc (*red*); MCCM-CCSD(T)-2sc (*green*); MCCM-CCSD(T)-2m (*blue*)

Table 1. Experimental and calculated KIEs at several temperatures for the reactions: CH_4/CD_4 + OH$\rightarrow$$CH_3/CD_3$ + H_2O/DOH

T(K)	1sc[a]	1sc[b]	2m[c]	2sc[d]	Exp[e]
200	3.66	7.45	8.85	8.58	
223	3.14	5.65	6.47	6.41	
298	2.38	3.30	3.57	3.65	7.36
300	2.36	3.27	3.68	3.61	
365	2.16	2.69	2.82	2.54	4.94
409	2.04	2.43	2.52	2.26	4.04
416	2.02	2.39	2.49	2.21	3.99
498	1.65	1.85	1.91	1.91	3.30
602	1.53	1.64	1.68	1.70	2.63
704	1.44	1.52	1.55	1.55	2.31
1000	1.30	1.34	1.34	1.37	
1500	1.12	1.13	1.14	1.16	

[a] MCCM-CCSD(T)-1sc (POLYRATE 8.5.1). [b] MCCM-CCSD(T)-1sc (POLYRATE 8.7). [c] MCCM-CCSD(T)-2sc (POLYRATE 8.7). [d] MCCM-CCSD(T)-2m (POLYRATE 8.7).
[e] From Ref. [1].

CD_4 + OH reaction, that is, we have not found a unique methodology that reproduces equally well the experimental rate constants for both title reactions.

In Table 1 the calculated KIEs at all the temperatures analyzed are compared to the experimental values at some particular temperatures. With the improved version of the code the calculated KIEs increase by a factor of 2.04 at 200 °K to a factor of 1.03 at 1000 °K (compare columns two and three of Table 1). Nevertheless, the theoretical KIEs calculated with the three different dynamical methodologies still underestimate the experimental results at all the temperatures. This underestimation in the calculated KIEs with the theoretical approaches that use corrected energies at the MCCM-CCSD(T)-1sc and the MCCM-CCSD(T)-2sc levels comes from the somewhat high values obtained for the deutero-isotopomer rate constants. In contrast, the MCCM-CCSD(T)-2m KIEs are small because the rate constants for the perprotio reaction are underestimated. Therefore, although we have achieved a significant improvement of the calculated KIEs of the title reaction, especially at low temperatures, it is clear that additional theoretical work is still needed to ameliorate them.

Acknowledgements. We thank DGESIC for financial support through Project No. PB98-0915. The use of the computational facilities of the CESCA and CEPBA coordinated by the C^4 is gratefully acknowledged.

References

1. Gordon S, Mulac WA (1975) Int J Chem Kinet 1:289; Baulch DL, Bowers M, Malcom DG, Tuckerman RT (1986) J Phys Chem Ref Data 15:465, and references therein; Atkinson R, (1989) J Phys Chem Ref Data 1:18; Vaghjiani GL, Ravishankara AR (1991) Nature (London) 350:406; Dunlop JR, Tully FP (1993) J Phys Chem 97:11148; DeMore WB (1993) J Phys Chem 97:8564; DeMore WB, Sander SP, Golden DM, Hampson RF, Kurylo MJ, Howard CJ, Ravishankara AR, Kolb CE, Molina MJ (1997) In: Chemical kinetics and photochemical data for use in stratospheric modeling. Evaluation number 12, jpl Publication 97-4, Jet Propulsion Laboratory, Pasadena, CA; Gierczak T, Talukdar RK, Herndon SC, Vaghjiani GL, Ravishankara AR (1997) J Phys Chem A 101:3125
2. Truong TN, Truhlar DG (1990) J Chem Phys 93:1761; Melissas VS, Truhlar DG (1993) J Chem Phys 99:1013; Melissas VS, Truhlar DG J Chem Phys (1993) 99:3542; Hu W-P, Liu Y-P, Truhlar DG (1994) J Chem Faraday Trans 90:1715; Dobbs KD, Dixon DA, Komornicki A (1993) J Chem Phys 98:8852; Schwartz M, Marshall P, Berry RJ, Ehlers CJ, Petersson GA (1998) J Phys Chem A 102:10074; Korchowiec J, Kawahara S, Matsumura K, Uchimaru T, Sugie M (1999) J Phys Chem A 103:3548; Espinosa-García J, Corchado JC (2000) J Chem Phys 112:5731; Masgrau L, González-Lafont A, Lluch JM (2001) J Chem Phys 114:2154; Masgrau L, González-Lafont A, Lluch JM (2001) J Chem Phys 115:4515
3. Allison TC, Truhlar DG (1998) In: Modern methods for multidimensional dynamics computations in chemistry. World Scientific, Singapore, p 618; Pu J, Corchado JC, Truhlar DG (2001) J Chem Phys 115:6266
4. Truhlar DG, Isaacson AD, Garrett BC (1985) In: Baer M (ed) Theory of chemical reaction dynamics. CRC, Boca Raton, vol IV, p 65
5. Tratz CM, Fast PL, Truhlar DG (1999) Phys Chem Comm 2:article 14, 1–10; Fast PL, Corchado JC, Sánchez ML, Truhlar DG (1999) J Phys Chem A 103:5129
6. Garrett BC, Truhlar DG, Grev RS, Magnuson AW (1980) J Phys Chem 84:1730; Garrett BC, Truhlar DG (1979) J Am Chem Soc 101:4534; Garrett BC, Truhlar DG (1979) J Am Chem Soc 101:5207
7. Liu Y-P, Lynch GC, Truong TN, Lu D-h, Truhlar DG, Garrett BC (1993) J Am Chem Soc 115:2408
8. Duncan WT, Bell RL, Truong TN (1998) J Comp Chem 19:1039; Chuang Y-Y, Corchado JC, Truhlar DG (1999) J Phys Chem A 103:1140
9. Villà J, Truhlar DG (1997) Theor Chem Acc 97:317
10. Corchado JC, Chuang Y-Y, Fast PL, Villà J, Hu W-P, Liu Y-P, Lynch GC, Nguyen KA, Jackels CF, Melissas VS, Lynch BJ, Rossi I, Coitiño EL, Fernández-Ramos A, Steckler R, Garrett BC, Isaacson AD, Truhlar DG (2000) POLYRATE 8.5.1. University of Minnesota, Minneapolis, (http://comp.chem.umn.edu/polyrate)
11. Corchado JC, Chuang Y-Y, Fast PL, Villà J, Hu W-P, Liu Y-P, Lynch GC, Nguyen KA, Jackels CF, Melissas VS, Lynch BJ, Rossi I, Coitiño EL, Fernández-Ramos A, Steckler R, Garrett BC, Isaacson AD, Truhlar DG (2001) POLYRATE 8.7. University of Minnesota, Minneapolis, (http://comp.chem.umn.edu/polyrate)

13 February 2002

ELSEVIER

Chemical Physics Letters 353 (2002) 154–162

CHEMICAL PHYSICS LETTERS

www.elsevier.com/locate/cplett

On the evaluation of quasi-thermodynamic magnitudes from rate constant values. Influence of the variational and tunnelling contributions

Laura Masgrau, Àngels González-Lafont, José M. Lluch *

Departament de Química, Universitat Autònoma de Barcelona, 08193 Bellaterra, Barcelona, Spain

Received 27 August 2001; in final form 10 December 2001

Abstract

Quasi-thermodynamic magnitudes obtained from three different analytical fits to the experimental rate constants of the $CH_4 + OH$ reaction are compared to the values obtained from theoretical rate constants calculated using canonical variational transition state theory plus multidimensional tunnelling contributions. A right decomposition of $\Delta G^{tot,0}$ into its enthalpic and entropic contributions is not experimentally feasible because it depends on the particular analytical expression used for the rate constants. Then, theoretical calculation of the rate constants at all the required temperatures becomes the only way to get reliable values of $\Delta H^{tot,0}$ (and E_a) and $\Delta S^{tot,0}$. Our results show that both variational and tunnelling nonsubstantial contributions to the quasi-thermodynamic magnitudes are significant for the $CH_4 + OH$ reaction and, probably, for a wide range of gas-phase chemical reactions.

1. Introduction

Determination of accurate values of gas-phase reaction rate constants is difficult both experimentally and theoretically. Likewise, the understanding of the main factors that govern their dependence on the temperature is not easy. To this aim, the very popular quasi-thermodynamic formulation of conventional transition state theory (TST) [1–3] is often used. Within this frame the rate constant is expressed in terms of quasi-thermodynamic magnitudes as

$$k(T) = \frac{k_B T}{h} K^0 e^{(-\Delta G^{\ddagger 0}/RT)} = \frac{k_B T}{h} K^0 e^{(\Delta S^{\ddagger 0}/R)} e^{(-\Delta H^{\ddagger 0}/RT)}, \quad (1)$$

where k_B is Boltzmann's constant, h is Planck's constant, K^0 is the quotient of the concentrations in the standard state (taken as 1 mol/l), and the three exponents contain, respectively, the standard-state activation Gibbs free energy, activation entropy and activation enthalpy (note that these three quantities depend on the temperature). According to TST, those magnitudes are evaluated

* Corresponding author. Fax: +34-935812920.
E-mail address: lluch@klingon.uab.es (J.M. Lluch).

0009-2614/02/$ - see front matter
PII: S0009-2614(01)01489-0

on the dividing surface that intersects the minimum energy path (MEP) [4,5] at the saddle point of the potential energy surface. Since the calculation is performed after elimination of the degree of freedom corresponding to the transition vector at the saddle point, those magnitudes are said to be quasi-thermodynamic quantities.

Experimental determination of those quasi-thermodynamic magnitudes allows us to make deductions about the nature of the transition state, serves to compare with other chemical reactions and to understand the reaction mechanism, and provides a good reference to test the goodness of the ab initio electronic structure calculations. However, evaluation of the quasi-thermodynamic magnitudes directly from the rate constants has to be made with great caution and their meaning is seldom simple. In this paper, we intend to illustrate this point taking the gas-phase hydrogen abstraction reaction from methane by hydroxyl radical as example. We have used several sets of available experimental rate constants at a range of temperatures, along with theoretical rate constants calculated in this Letter by means of a direct dynamics multicoefficient method that we have very recently proven to provide accurate enough rate constants for most of the practical applications [6].

2. Method of calculation

Canonical variational transition (CVT) state theory [7,8] plus multidimensional tunnelling (MT) contributions have been used to calculate the rate constants for the $CH_4 + OH$ reaction in the interval 200–1500 K. The small-curvature tunnelling (SCT) semiclassical adiabatic ground-state approximation [9] has been used to correct for tunnelling. The SCT approximation is appropriate for the $CH_4 + OH$ reaction because, as shown by Truhlar and coworkers [10], the small-curvature tunneling mechanism is dominant at all energies for this reaction. The CVT/SCT rate constant is given by

$$k^{\mathrm{CVT/SCT}}(T,s_*) = \kappa^{\mathrm{tun}}(T)\frac{\sigma k_{\mathrm{B}}T}{h}\frac{Q^{\mathrm{GT}}(T,s_*)}{Q^{\mathrm{R}}(T)} \times \exp(-V_{\mathrm{MEP}}(s_*)/k_{\mathrm{B}}T), \qquad (2)$$

where $\kappa^{\mathrm{tun}}(T)$ is the SCT transmission coefficient, s_* denotes the value of s at the free energy maximum along the MEP at temperature T, σ is the symmetry factor [11] (taken as 12 for the present reaction), $Q^{\mathrm{R}}(T)$ and $Q^{\mathrm{GT}}(T,s_*)$ are the reactants and the generalized transition state partition functions per unit volume, respectively, excluding symmetry numbers for rotation, and $V_{\mathrm{MEP}}(s_*)$ is the classical potential energy at s_*.

The electronic structure information from the potential energy surface (PES) needed for carrying out these dynamical calculations has been taken from our previous work (see Tables 1 and 2 in [6]) on the $CH_4 + OH$ reaction and several of its isotope variants [6]. In that work, we showed that the so-called MCCM-CCSD(T)-1sc multilevel single-point energy scheme provides theoretical rate constants in good agreement with the experimental rate constants for the set of reactions studied. MCCM stands for multicoefficient correlation methods [12,13] and CCSD(T) stands for the coupled cluster method including single and double excitations and a perturbative estimate of the effect of triple excitations [14] (the meaning of the 1sc acronym will be explained below). MCCM methods are new methodologies, within the field of general parametrization for semiempirical extrapolation approaches, that attempt to extrapolate to the full configuration limit and to reach the infinite-basis limit. In particular, we used the MCCM-CCSD(T) scheme in its Colorado version [13], which gives a single-point energy equal to

$$\begin{aligned} E[\mathrm{MCCM\text{-}CCSD(T)}] &= c_1 E(\mathrm{HF/cc\text{-}pVDZ}) \\ &+ c_2 \Delta E(\mathrm{HF/cc\text{-}pVTZ}|\mathrm{cc\text{-}pVDZ}) \\ &+ c_3 \Delta E(\mathrm{MP2}|\mathrm{HF/cc\text{-}pVDZ}) \\ &+ c_4 \Delta E(\mathrm{MP2}|\mathrm{HF/cc\text{-}pVTZ}|\mathrm{cc\text{-}pVDZ}) \\ &+ c_5 \Delta E(\mathrm{CCSD}|\mathrm{MP2/cc\text{-}pVDZ}) \\ &+ c_6 \Delta E(\mathrm{CCSD}|\mathrm{MP2/cc\text{-}pVTZ}|\mathrm{cc\text{-}pVDZ}) \\ &+ c_7 \Delta E(\mathrm{CCSD(T)}|\mathrm{CCSD/cc\text{-}pVDZ}) \\ &+ c_8 \Delta E(\mathrm{CCSD(T)}|\mathrm{CCSD/cc\text{-}pVTZ}|\mathrm{cc\text{-}pVDZ}) \\ &+ E_{\mathrm{SO}} + E_{\mathrm{CC}}, \end{aligned} \qquad (3)$$

where

$$\Delta E(M_1\,|\,M_2/B) = E(M_1/B) - E(M_2/B),$$
$$\Delta E(M_1/B_1\,|\,B_2) = E(M_1/B_1) - E(M_1/B_2),$$
$$\Delta E(M_1\,|\,M_2/B_1\,|\,B_2) = [E(M_1/B_1) - E(M_2/B_1)] - [E(M_1/B_2) - E(M_2/B_2)],$$

where (M and B indicate electronic method and basis set, respectively) cc-pVDZ and cc-pVTZ stand for Dunning's correlation-consistent polarized-valence double zeta and triple zeta basis sets [15], respectively, both with pure d and f functions; c_i are coefficients and CCSD is the notation for the coupled cluster method including single and double excitations. E_{SO} and E_{CC} are the spin–orbit [16] and core-correlation [17] contributions, respectively. The 1sc notation means that these two energetic terms are included explicitly, as in Eq. (3). However, we used the 1sc set of coefficients omitting the E_{CC} term in Eq. (3) but calculating the single-point energies with a full electron correlation treatment. For the spin–orbit contribution we have taken $E_{SO} = -0.2$ kcal/mol for the hydroxyl radical and $E_{SO} = 0.0$ for the other stationary points and along the MEP, as they are closed-shell molecules or doublet molecules in the ^{2}A state, which have E_{SO} necessarily zero in the Russell–Saunders scheme. Number 1 indicates that the coefficients were optimized to get accurate atomization energy values of a 49-molecule data set [16].

For the MCCM calculations stationary point geometries, first and second derivatives at second-order Möller–Plesset perturbation theory [18,19] (MP2) based on restricted Hartree–Fock (RHF) or unrestricted Hartree–Fock (UHF) wave functions for closed-shell and open-shell systems, respectively, and with a full electron correlation treatment, have been taken from our previous work [6] on the $CH_4 + OH$ reaction. The basis set used in that paper, and also adopted here, was the cc-pVTZ basis set of Dunning with pure d and f functions. The low level MEP has also been taken from our previous paper. It consists in a total of 35 nonstationary points (geometries, gradients and hessians), calculated at the MP2(full)/cc-pVTZ level of theory, from $s = -2.20$ to 0.50 bohr (where s denotes the distance along the MEP in an isonertial mass-scaled coordinate system with a scaling mass equal to 1 amu, with $s = 0$ at the saddle point, s negative on the reactant side of the saddle point and positive on the product side). Single-point energy calculations at the MCCM-CCSD(T) level with a full electron correlation treatment were made at a small number of nonstationary point geometries along the MP2(full)/cc-pVTZ MEP, to correct the classical energy profile for the dynamical calculations. The location of five of these points along the MEP corresponds to the one chosen in our previous work, that is at s values of −0.900, −0.200, −0.051, +0.031 and +0.051 bohr.

All the energy calculations and the geometry optimizations were carried out with the GAUSSIAN 94 system of programs [20].

For the dynamical calculations carried out in this work, we have chosen a dual-level direct dynamics approach known as the interpolated single-point energy (ISPE) correction [21,22] algorithm. Following the ISPE procedure, the MP2(full)/cc-pVTZ geometries and frequencies, scaled by 0.9790 [16,23], at the stationary points and along the MEP have been used as the low level (LL) electronic structure information of the PES. Then, MCCM-CCSD(T) classical single-point energies calculated at the stationary points and at the nonstationary points mentioned above, have been used as the high level (HL) information to correct for the energetics.

As in our previous work, the re-oriented dividing surface (RODS) [24] algorithm has been applied in order to improve the generalized frequencies along the low level MEP. The normal mode analysis has been performed in redundant internal coordinates [25] (six stretches, eight bends and four torsions). All vibrations have been treated within the harmonic approximation except the internal rotational motion corresponding to the lowest mode at the saddle point and along the MEP, which has been treated as a hindered rotor [26] (see our previous paper [6] for details). We have assumed no low-lying excited state of the $^2A_1$ saddle point, but we have included the $^2\Pi_{1/2}$ excited state (140 cm^{-1}) for OH, in the electronic partition functions.

We have used the POLYRATE 8.5.1 code [27] for all the dynamical calculations.

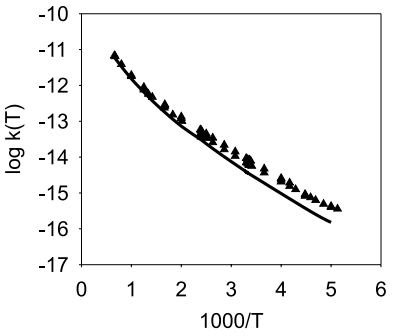

Fig. 1. Arrhenius plots of the experimental (triangles) and MCCM-CCSD(T)-1sc calculated (solid line) rate constants. Rate constants are in cm^3 $molecule^{-1}$ s^{-1} and temperatures in Kelvin.

In order to show the goodness of our CVT/SCT rate constants we have compared them with the corresponding experimental rate constants (see Fig. 1).

3. Results and discussion

The first aspect that has to be considered is that for many reactions variational effects are important, in such a way that the variational transition state (that is, the kinetic bottleneck of the reaction) is no longer located at the saddle point, but it moves along the MEP depending on the temperature. In addition, in reactions where the main chemical change consists of the jump of light nuclei the tunnelling effect has to be taken into account. In this case, Eq. (1) has to be modified in order to introduce the transmission coefficients $\kappa_{\rm tun}(T)$ and $\kappa_{\rm var}(T)$, which accounts for the tunnelling and variational effects, respectively:

$$k(T) = \kappa_{\rm tun}(T)\kappa_{\rm var}(T)\frac{k_{\rm B}T}{h}K^0 e^{(-\Delta G^{\ddagger 0}/RT)} = \kappa_{\rm tun}(T)\kappa_{\rm var}(T)\frac{k_{\rm B}T}{h}K^0 e^{(\Delta S^{\ddagger 0}/R)}e^{(-\Delta H^{\ddagger 0}/RT)}. \quad (4)$$

Note that $\kappa_{\rm tun}(T) \geqslant 1$, but $\kappa_{\rm var}(T)$, defined as the ratio between the CVT (no tunnelling included) and the TST rate constants, is equal or smaller than 1. However, sometimes the rate constants are fitted still maintaining the shape of Eq. (1). When this is the case, one has to realize that $\Delta G^{\rm tot,0}, \Delta H^{\rm tot,0}$ and $\Delta S^{\rm tot,0}$ are actually obtained as quasi-thermodynamic magnitudes, instead of $\Delta G^{\ddagger 0}, \Delta H^{\ddagger 0}$ and $\Delta S^{\ddagger 0}$. Those 'total' quantities arise from formally incorporating the effect of $\kappa_{\rm tun}(T)$ and $\kappa_{\rm var}(T)$ into $\Delta G^{\ddagger 0}, \Delta H^{\ddagger 0}$ and $\Delta S^{\ddagger 0}$ in Eq. (4):

$$k(T) = \frac{k_{\rm B}T}{h}K^0 e^{(-\Delta G^{\rm tot,0}/RT)} = \frac{k_{\rm B}T}{h}K^0 e^{(\Delta S^{\rm tot,0}/R)}e^{(-\Delta H^{\rm tot,0}/RT)}. \quad (5)$$

As a matter of fact, Eq. (1) just holds when tunnelling and variational effects are negligible.

Taking all that into account, we have chosen a discrete set of experimental rate constants taken from Ravishankara and coworkers [28] (195 K $\leqslant T \leqslant$ 298 K), Vaghjiani and Ravishankara [29] (300 K $\leqslant T \leqslant$ 420 K), and Atkinson [30] (500 K $\leqslant T \leqslant$ 1512 K) Using Eq. (5) we have plotted $k(T)/T$ against $1/T$ looking for the least-squares best linear fitting. The corresponding straight line, with a good correlation coefficient $\rho = -0.994$, provides the values 3.49 kcal/mol and −16.33 cal/(mol K) for $\Delta H^{\rm tot,0}$ and $\Delta S^{\rm tot,0}$, respectively. These values have been obtained assuming that both $\Delta H^{\rm tot,0}$ and $\Delta S^{\rm tot,0}$ are independent on the temperature, in such a way that the above fitting leads to a real straight line. Since this is not true, the correct procedure involves two steps: first, $\Delta G^{\rm tot,0}(T)$ is calculated from $k(T)$ at each given temperature using Eq. (5); second, by using the van't Hoff equation, $\Delta G^{\rm tot,0}(T)$ is decomposed into the enthalpic and the entropic contributions through equations (for a bimolecular gas-phase reaction)

$$\Delta H^{\rm tot,0}(T) = -T^2\frac{{\rm d}(\Delta G^{\rm tot,0}(T)/T)}{{\rm d}T} - RT \quad (6)$$

and

$$\Delta S^{\rm tot,0}(T) = \frac{\Delta H^{\rm tot,0}(T) - \Delta G^{\rm tot,0}(T)}{T}. \quad (7)$$

These equations are equivalent to those employed previously by Truhlar and Garrett [31]. In practice, we have calculated the numerical derivatives in Eq. (6) by a three-point central difference algorithm. However, the discrete set of experimental rate constants we have used above is not dense enough to provide accurate derivatives (this

will be always the scenario, unless a huge number of experimental measurements at very close temperatures is made). Then, we need a continuous function $k(T)$. Continuous expressions are usually obtained by fitting of suitable functions to the experimental rate constants. Many authors employ the three-parameter expression

$$k(T) = BT^n e^{(-E/T)}. \quad (8)$$

Note that the parameters B and E of Eq. (8) do not coincide with the preexponential factor A and the activation energy E_a/R corresponding to an Arrhenius equation, unless $n = 0$. For the $CH_4 + OH$ reaction many three-parameter fits of that type exist. In this Letter, we have selected three of them (in all cases the rate constants are given in cm^3 $molecule^{-1}$ s^{-1}):

1. From the Atkinson data [30] ($500\ K \leqslant T \leqslant 1512\ K$). $B = 6.95 \times 10^{-18}$; $n = 2$; $E = 1282$.
2. From Baulch et al. [32] ($240\ K \leqslant T \leqslant 2500\ K$). $B = 2.57 \times 10^{-17}$; $n = 1.83$; $E = 1396$.
3. The fit recommended by the data evaluation panel NASA/JPL [33] ($200\ K \leqslant T \leqslant 420\ K$). $B = 2.80 \times 10^{-14}$; $n = 0.667$; $E = 1575$.

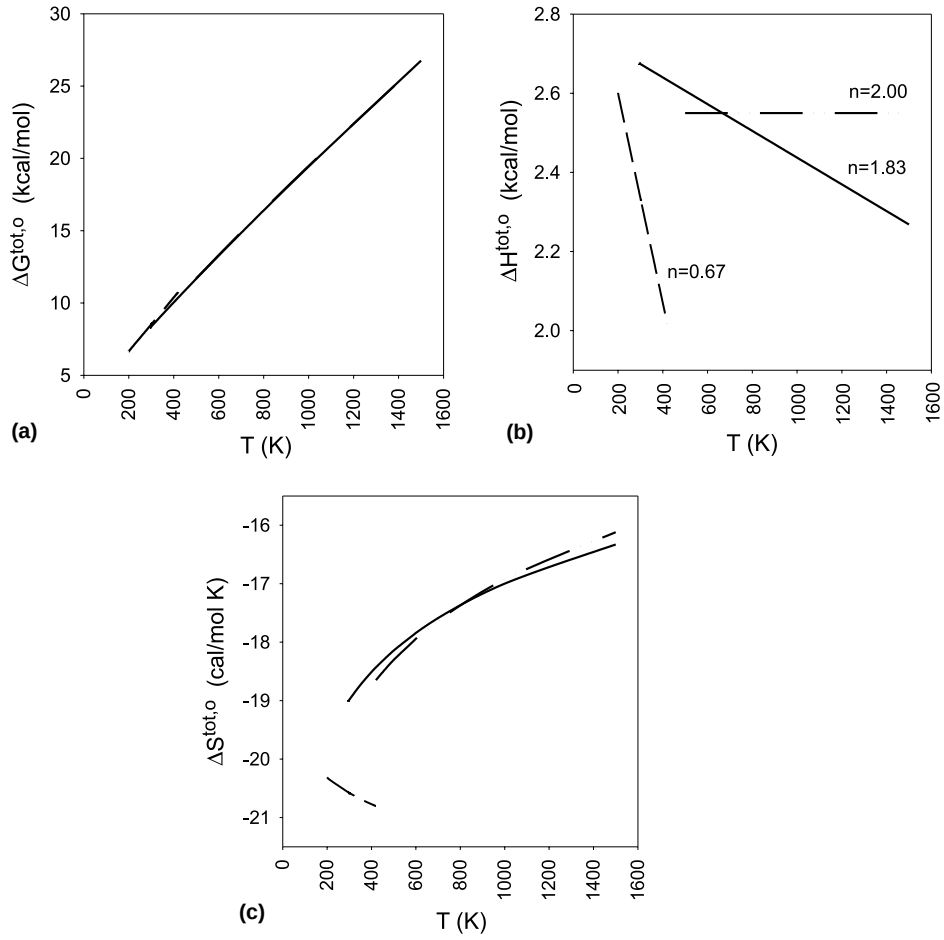

Fig. 2. (a) Experimental $\Delta G^{tot,0}$ values as a function of temperature: values derived from [30] (dashed–dotted–dotted line); values derived from [32] (solid line); values derived from [33] (dashed–dashed line); (b) $\Delta H^{tot,0}$ contribution as a function of temperature calculated with Eq. (6): values derived from [30] (dashed–dotted–dotted line); values derived from [32] (solid line); values derived from [33] (dashed–dashed line); (c) $\Delta S^{tot,0}$ contribution as a function of temperature calculated with Eq. (7): values derived from [30] (dashed–dotted–dotted line); values derived from [32] (solid line); values derived from [33] (dashed–dashed line).

Then, we have used these three analytical fits along with Eqs. (5)–(7) to obtain $\Delta G^{tot,0}$, $\Delta H^{tot,0}$ and $\Delta S^{tot,0}$. The results are pictured in Fig. 2. It can be seen (Fig. 2a) that the $\Delta G^{tot,0}$ values derived from the Atkinson's [30] and Baulch's [32] fits match, the NASA's [33] fit deviating very slightly from the Baulch's [32] fit (note that Fig. 2a does not contain a straight line in spite that it would look like it at first glance). The good agreement between the three cases reflects the fact that there is a biunivocal correspondence between the $k(T)$ and $\Delta G^{tot,0}$ values through Eq. (5). As a consequence, if the three fits correspond to very similar rate constant values, they have to lead to very similar $\Delta G^{tot,0}$ values. The scenario turns out to be drastically different for their enthalpic (Fig. 2b) and entropic (Fig. 2c) contributions. In effect, rather surprisingly, three entirely different straight lines are obtained for $\Delta H^{tot,0}$. Several points merit to be remarked observing Fig. 2b: (a) $\Delta H^{tot,0}$ exhibits a clear dependence on the temperature in two of the cases; (b) the above value (3.49 kcal/mol) obtained by least-square linear fitting has nothing to do with the range of values obtained through Eq. (6); and (c) the values of $\Delta H^{tot,0}$ depend on which is the particular fit we have employed. It can be easily shown that the functions given in Eq. (8) lead to linear plots of $\Delta H^{tot,0}$ versus T, with a slope equal to $(n-2)R$ (so, for $n=2$ $\Delta H^{tot,0}$ becomes independent on the temperature!). On the other hand, $\Delta S^{tot,0}$ also depends clearly on the temperature, the value (−16.33 cal/mol K) obtained from the above least-square linear fitting is quite far from the values shown in Fig. 2c, and different fits lead to different $\Delta S^{tot,0}$ values.

At this point, we can conclude that a right decomposition of $\Delta G^{tot,0}$ into its enthalpic and entropic components from analytical fits to the experimental rate constants is not feasible, because many different fits are possible and each one preserves the actual values of $\Delta G^{tot,0}$, but each one leads to radically different partitions of them into their $\Delta H^{tot,0}$ and $\Delta S^{tot,0}$ contributions. It has to be emphasize that for a bimolecular gas-phase reaction the relationship $E_a = \Delta H^{tot,0} + 2RT$ holds. Therefore, analytical fits that lead to wrong values of $\Delta H^{tot,0}$ provide wrong values of the activation energy as well. Then, theoretical calculation of the rate constants at all the required temperatures to evaluate the corresponding derivatives becomes the only way to get reliable values of $\Delta H^{tot,0}$ (and E_a) and $\Delta S^{tot,0}$. Following this idea, we have first calculated the rate constants at a range of temperatures according to the procedure outlined in Section 2, and, second, we have applied Eqs. (5)–(7) to the theoretical rate constants. It has to be remarked that three theoretical rate constants at very close temperatures have to be calculated for each temperature at which the results are presented.

Table 1
From left to right, as a function of the temperature: conventional rate constants, variational rate constants, variational rate constants including tunneling, total activation Gibbs free energy (in kcal/mol), total activation enthalpy (in kcal/mol) and total activation entropy (in cal/mol K)

T (K)	k^{TST}	k^{CVT}	$k^{CVT/SCT}$	$\Delta G^{tot,0}$	$\Delta H^{tot,0}$	$\Delta S^{tot,0}$
200	1.05(−15)	1.81(−17)	1.51(−16)	7.01	2.57	−22.22
223	2.61(−15)	6.98(−17)	3.74(−16)	7.47	2.74	−21.20
298	1.98(−14)	1.39(−15)	3.45(−15)	8.83	3.02	−19.51
300	2.06(−14)	1.47(−15)	3.61(−15)	8.87	3.02	−19.48
350	5.00(−14)	5.34(−15)	1.03(−14)	9.73	3.12	−18.89
400	1.00(−13)	1.43(−14)	2.36(−14)	10.56	3.17	−18.48
420	1.27(−13)	2.01(−14)	3.14(−14)	10.89	3.18	−18.36
500	2.82(−13)	5.92(−14)	7.31(−14)	12.30	3.19	−18.23
600	6.04(−13)	1.58(−13)	1.80(−13)	13.90	3.21	−17.82
700	1.10(−12)	3.34(−13)	3.63(−13)	15.46	3.29	−17.39
1000	3.98(−12)	1.50(−12)	1.53(−12)	19.93	3.43	−16.51
1500	1.49(−11)	6.29(−12)	5.87(−12)	27.10	3.86	−15.49

Rate constants are given in cm^3 $molecule^{-1}$ s^{-1} (power of 10 in parentheses).

The conventional rate constants (k^{TST}), variational rate constants (k^{CVT}) and variational rate constants including tunnelling ($k^{CVT/SCT}$) are given from the second to fourth columns in Table 1. Ratios between $k^{CVT}(T)$ and $k^{TST}(T)$ provide $\kappa_{var}(T)$, whereas ratios between $k^{CVT/SCT}(T)$ and $k^{CVT}(T)$ give $\kappa_{tun}(T)$. It can be seen that variational effects and tunnelling corrections are very important at low temperatures (they change the rate constants by two orders or one order of magnitude, respectively, at 200 K). On the other hand, the higher the temperature the smaller both variational effects and tunnelling corrections become. At 1500 K, $k^{CVT/SCT}$ is slightly smaller than k^{CVT} because the ratio of the Boltzmann average of the classical transmission probability with the threshold energy at the maximum of the adiabatic ground-state energy to the Boltzmann average of the classical transmission probability with the threshold energy at s_*, is smaller than one.

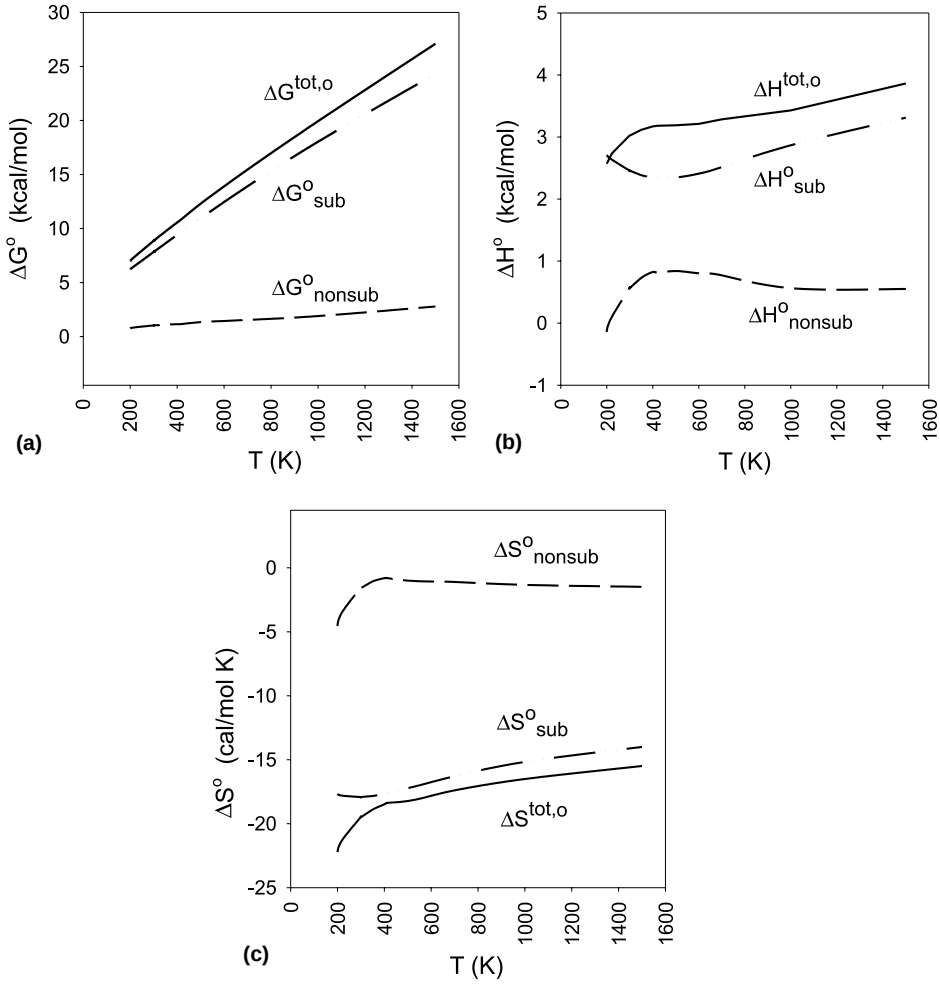

Fig. 3. (a) Theoretical $\Delta G^{tot,0}$ values as a function of temperature (solid line) and temperature dependence of its two contributions: ΔG^0_{sub} (dashed–dotted–dotted line) and ΔG^0_{nonsub} (dashed–dashed line); (b) theoretical $\Delta H^{tot,0}$ values as a function of temperature (solid line) and temperature dependence of its two contributions: ΔH^0_{sub} (dashed–dotted–dotted line) and ΔH^0_{nonsub} (dashed–dashed line); (c) theoretical $\Delta S^{tot,0}$ values as a function of temperature (solid line) and temperature dependence of its two contributions: ΔS^0_{sub} (dashed–dotted–dotted line) and ΔS^0_{nonsub} (dashed–dashed line).

$\Delta G^{\mathrm{tot},0}(T)$, $\Delta H^{\mathrm{tot},0}(T)$ and $\Delta S^{\mathrm{tot},0}(T)$ derived from $k^{\mathrm{CVT/SCT}}(T)$ are presented in the last three columns, respectively, in Table 1. Likewise, they are pictured in Fig. 3. $\Delta H^{\mathrm{tot},0}$ increases as temperature augments, and its corresponding plot is not a straight line at all. Then, the values and trends of the theoretical $\Delta H^{\mathrm{tot},0}$ are very different from the ones corresponding to $\Delta H^{\mathrm{tot},0}$ obtained from the experimental rate constants. It has to be remarked that this disagreement is not due to discrepancies between the theoretical and the experimental rate constants, but to the fact that the available experimental rate constants do not contain the suitable information to determine $\Delta H^{\mathrm{tot},0}$. Indeed the same consideration is valid in order to determine $\Delta S^{\mathrm{tot},0}$.

Another important problem concerns to the real meaning of the 'total' quasi-thermodynamic magnitudes. As stated above, they include several different effects. According to Truhlar and Garrett [31], $\Delta H^{\mathrm{tot},0}$ can be partitioned into substantial ($\Delta H^{\ddagger 0} = \Delta H^{0}_{\mathrm{sub}}$) and nonsubstantial ($\Delta H^{0}_{\mathrm{nonsub}}$) contributions. The former arises from properties of a single temperature-independent transition state attached to the saddle point. The nonsubstantial contributions come from the dependence of the variational transition state on temperature ($\Delta H^{\mathrm{var},0}$) and tunnelling effects ($\Delta H^{\mathrm{tun},0}$). The same can be said regarding $\Delta G^{\mathrm{tot},0}$ and $\Delta S^{\mathrm{tot},0}$. Whatever attempt to interpret the values and dependence on the temperature of the rate constants requires such a decomposition, which can be made by means of

$$\begin{aligned}\Delta G^{\mathrm{tot},0}(T) &= \Delta G^{\ddagger 0}(T) + \Delta G^{\mathrm{var},0}(T) + \Delta G^{\mathrm{tun},0}(T)\\ &= \Delta G^{\ddagger 0}(T) - RT\ln\kappa_{\mathrm{var}}(T)\\ &\quad - RT\ln\kappa_{\mathrm{tun}}(T),\end{aligned} \tag{9}$$

$$\begin{aligned}\Delta H^{\mathrm{tot},0}(T) &= \Delta H^{\ddagger 0}(T) + \Delta H^{\mathrm{var},0}(T) + \Delta H^{\mathrm{tun},0}(T)\\ &= \Delta H^{\ddagger 0}(T) + RT^2\frac{\mathrm{d}\ln\kappa_{\mathrm{var}}(T)}{\mathrm{d}T}\\ &\quad + RT^2\frac{\mathrm{d}\ln\kappa_{\mathrm{tun}}(T)}{\mathrm{d}T},\end{aligned} \tag{10}$$

$$\begin{aligned}\Delta S^{\mathrm{tot},0}(T) &= \Delta S^{\ddagger 0}(T) + \Delta S^{\mathrm{var},0}(T) + \Delta S^{\mathrm{tun},0}(T)\\ &= \Delta S^{\ddagger 0}(T) + RT\frac{\mathrm{d}\ln\kappa_{\mathrm{var}}(T)}{\mathrm{d}T} + R\ln\kappa_{\mathrm{var}}(T)\\ &\quad + RT\frac{\mathrm{d}\ln\kappa_{\mathrm{tun}}(T)}{\mathrm{d}T} + R\ln\kappa_{\mathrm{tun}}(T).\end{aligned} \tag{11}$$

As seen, evaluation of enthalpic and entropic nonsubstantial contributions requires numerical derivatives of the transmission coefficients (from theoretical calculations). The results are shown in Table 2 and Fig. 3. We see that substantial activation enthalpy exhibits a small variation with temperature. It has to be recalled that $\Delta H^{\ddagger 0}$ comes from the classical energy barrier at the saddle point plus zero-point energy and thermal corrections. Slight differences on these thermal corrections produces the small variations of $\Delta H^{\ddagger 0}$. On the other hand, it is clear that for the $CH_4 + OH$ reaction both contributions to the nonsubstantial activation enthalpy are remarkable (in the previous cases studied by Truhlar and Garrett [31], the important

Table 2
Substantial, variational and tunnelling contributions to the activation enthalpies (in kcal/mol) and entropies (in cal/mol K) as a function of the temperature

T (K)	$\Delta H^{\ddagger 0}$	$\Delta H^{\mathrm{var},0}$	$\Delta H^{\mathrm{tun},0}$	$\Delta S^{\ddagger 0}$	$\Delta S^{\mathrm{var},0}$	$\Delta S^{\mathrm{tun},0}$
200	2.71	1.69	−1.83	−17.67	0.40	−4.95
223	2.63	1.69	−1.59	−17.82	0.41	−3.80
298	2.46	1.69	−1.14	−17.92	0.40	−2.00
300	2.46	1.68	−1.11	−17.92	0.35	−1.91
350	2.38	1.66	−0.93	−17.83	0.31	−1.37
400	2.35	1.63	−0.80	−17.67	0.21	−1.02
420	2.36	1.58	−0.76	−17.53	0.09	−0.92
500	2.35	1.38	−0.54	−17.22	−0.34	−0.66
600	2.41	1.26	−0.46	−16.75	−0.56	−0.51
700	2.52	1.12	−0.35	−16.28	−0.77	−0.34
1000	2.87	0.86	−0.29	−15.17	−1.09	−0.25
1500	3.31	0.40	0.15	−14.00	−1.46	−0.03

contributions were only due to tunnelling), specially at low temperatures. $\Delta H^{var,0}$ turns out to be positive due to the fact that for the $CH_4 + OH$ reaction the variational effect become more significant at low temperatures. This way, in this case, both nonsubstantial components exert opposite effects. For a reaction in which variational effects appear specially at higher temperatures, the influence of variational and tunnelling contributions will reinforce. As for the activation entropy, the main component is the substantial one.

To summarize, in this Letter we have shown that important information can be obtained from the analysis of the quasi-thermodynamic magnitudes deduced from theoretical rate constants. However, a quasi-thermodynamic analysis based on experimental rate constants can be misleading and it is not recommended, specially if the studied reaction undergoes non-negligible variational and/or tunnelling effects. On the other hand, it has to be pointed that both variational and tunnelling nonsubstantial contributions to the quasi-thermodynamic magnitudes are significant for the $CH_4 + OH$ reaction and, probably, for a wide range of gas-phase chemical reactions.

Acknowledgements

Financial support from the Dirección General de Enseñanza Superior (DGES) through project PB98-0915 and the use of the computational facilities of the CESCA and CEPBA coordinated by the C^4 are gratefully acknowledged.

References

[1] S. Glasstone, K.J. Laidler, H. Eyring, The Theory of Rate Processes, McGraw-Hill, New York, 1941.
[2] S.W. Benson, Thermochemical Kinetics, second ed., Wiley, New York, 1976.
[3] J.I. Steinfeld, J.S. Francisco, W.L. Hase, Chemical Kinetics and Dynamics, Prentice-Hall, New Jersey, 2000.
[4] D.G. Truhlar, A. Kupperman, J. Am. Chem. Soc. 93 (1971) 1840.
[5] K. Fukui, Pure Appl. Chem. 54 (1982) 1825.
[6] L. Masgrau, A. González-Lafont, J.M. Lluch, J. Chem. Phys. 115 (2001) 4515.
[7] D.G. Truhlar, A.D. Isaacson, B.C. Garrett, in: M. Baer (Ed.), Theory of Chemical Reaction Dynamics, vol. IV, CRC Press, Boca Raton, FL, 1985, p. 65.
[8] S.C. Tucker, D.G. Truhlar, in: J. Bertrán, I.G. Csizmadia (Eds.), New Theoretical Concepts for Understanding Organic Reactions, Kluwer Academic Publishers, Dordrecht, 1989, p. 291.
[9] Y.-P. Liu, G.C. Lynch, T.N. Truong, D.-h. Lu, D.G. Truhlar, B.C. Garrett, J. Am. Chem. Soc. 115 (1993) 2408.
[10] W.-P. Hu, Y.-P. Liu, D.G. Truhlar, J. Chem. Soc., Faraday Trans. 90 (1994) 1715.
[11] P. Pechukas, J. Chem. Phys. 64 (1976) 1516.
[12] C.M. Tratz, P.L. Fast, D.G. Truhlar, Phys. Chem. Comm. 2/article 14 (1999) 1.
[13] P.L. Fast, J.C. Corchado, M.L. Sánchez, D.G. Truhlar, J. Phys. Chem. A 103 (1999) 5129.
[14] K. Raghavachari, G.W. Trucks, J.A. Pople, M. Head-Gordon, Chem. Phys. Lett. 157 (1989) 479.
[15] T.H. Dunning Jr., J. Chem. Phys. 90 (1989) 1007.
[16] L. Fast, J.C. Corchado, M.L. Sánchez, D.G. Truhlar, J. Phys. Chem. A 103 (1999) 3139.
[17] P.L. Fast, D.G. Truhlar, J. Phys. Chem. A 103 (1999) 3802.
[18] W.J. Hehre, L. Radom, P.v.R. Schleyer, J.A. Pople, Ab Initio Molecular Orbital Theory, Wiley, New York, 1986.
[19] C. Møller, M.S. Plesset, Phys. Rev. 46 (1934) 618.
[20] M.J. Frisch et al., GAUSSIAN 94, Gaussian Inc., Pittsburgh, PA, 1995.
[21] W.T. Duncan, R.L. Bell, T.N. Truong, J. Comp. Chem. 19 (1998) 1039.
[22] Y.-Y. Chuang, J.C. Corchado, D.G. Truhlar, J. Phys. Chem. A 103 (1999) 1140.
[23] A.P. Scott, L. Radom, J. Phys. Chem. 100 (1996) 16502.
[24] J. Villà, D.G. Truhlar, Chem. Theor. Acc. 97 (1997) 317.
[25] Y.-Y. Chuang, D.G. Truhlar, J. Phys. Chem. A 102 (1998) 242.
[26] Y.-Y. Chuang, D.G. Truhlar, J. Chem. Phys. 112 (2000) 1221.
[27] J.C. Corchado et al., POLYRATE 8.5.1, University of Minnesota, Minneapolis, MN, 2000 (available from: http://comp.chem.umn.edu/polyrate).
[28] T. Gierczak, R.K. Talukdar, S.C. Herndon, G.L. Vaghjiani, A.R. Ravishankara, J. Phys. Chem. A 101 (1997) 3125.
[29] G.L. Vaghjiani, A.R. Ravishankara, Nature(London) 350 (1991) 406.
[30] R. Atkinson, J. Phys. Chem. Ref. Data 1 (1989) 18.
[31] D.G. Truhlar, B.C. Garrett, J. Am. Chem. Soc. 111 (1989) 1232.
[32] D.L. Baulch, C.J. Cobos, R.A. Cox, C. Esser, P. Frank, T. Just, J.A. Kerr, M.J. Pilling, J. Troe, R.W. Walker, J. Warnatz, J. Phys. Chem. Ref. Data 21 (1992) 411.
[33] W.B. DeMore, S.P. Sander, D.M. Golden, R.F. Hampson, M.J. Kurylo, C.J. Howard, A.R. Ravishankara, C.E. Kolb, M.J. Molina, Chemical Kinetics and Photochemical Data for use in Stratospheric Modeling, Evaluation Number 12, JPL Publication 97-4, Jet Propulsion Laboratory, California Institute of Technology, Pasadena, CA, 1997.